License R-23
Docket 50-2

MICHIGAN MEMORIAL PHOENIX PROJECT
THE UNIVERSITY OF MICHIGAN

SAFETY ANALYSIS

UTILIZATION OF LOW ENRICHMENT URANIUM (LEU) FUEL IN THE FORD NUCLEAR REACTOR

FORD NUCLEAR REACTOR
MICHIGAN MEMORIAL - PHOENIX PROJECT
THE UNIVERSITY OF MICHIGAN
Ann Arbor

October, 1979

Prepared For
U.S. Nuclear Regulatory Commission

ANN ARBOR MICHIGAN

SAFETY ANALYSIS

UTILIZATION OF LOW ENRICHMENT URANIUM (LEU) FUEL IN THE FORD NUCLEAR REACTOR

FORD NUCLEAR REACTOR
MICHIGAN MEMORIAL-PHOENIX PROJECT
THE UNIVERSITY OF MICHIGAN
Ann Arbor

October , 1979

ABSTRACT

This analysis reviews the safety aspects of utilizing low enrichment uranium (LEU-less than 20% enrichment) fuel in the Ford Nuclear Reactor (FNR). A brief description of the proposed fuel is followed by an examination of fuel swelling, high temperature blistering, and failure data for similar operational and test fuels under operating conditions similar to those in the FNR. Fuel specifications have been developed with technical requirements identical to those for reactors which use equivalent fuel. Heat transfer characteristics are not examined in detail because fuel and coolant flow channel dimensions are identical to those in present FNR fuel. Core physics analyses show some variation in fast and thermal neutron flux distributions within the core and in the reflector regions. The available data and the analyses performed indicate that no reduction in safety margins are expected from utilizing LEU fuel in the FNR core.

TABLE OF CONTENTS

		Page
TITLE PAGE		
ABSTRACT		i
TABLE OF CONTENTS		ii
1.	INTRODUCTION	1
2.	FUEL DESCRIPTION	1
3.	OPERATING CONDITIONS	2
4.	FUEL CORE SWELLING	2
5.	FUEL CORE BLISTERING	2
6.	FAILURE HISTORY	13
7.	FUEL SPECIFICATIONS	13
8.	HEAT TRANSFER CHARACTERISTICS	15
9.	CORE PHYSICS	16
10.	DEMONSTRATION EXPERIMENT AND MEASUREMENT PROGRAM	48

LIST OF FIGURES

Figure 1	Fuel Core Swelling	7
Figure 2	Fuel Core Blister Temperature	12
Figure 3	Fuel Burnup Distribution for FNR Cycle 67	23
Figure 4	Experimental and Calculated Power Distributions for FNR Cycle 67	25
Figure 5	Fuel Burnup Distribution for FNR Cycle 163B	26
Figure 6	Experimental and Calculated Thermal Flux Distributions for FNR Cycle 163B	27
Figure 7	Batch Core Configuration	29
Figure 8	Equilibrium Core Loading Pattern	31
Figure 9	Assembly Power Distribution for Batch Core	41
Figure 10	Assembly Power Distribution for Equilibrium Core	42
Figure 11	Assembly-Average Thermal Flux Distribution for Batch Core	43
Figure 12	Assembly-Average Thermal Flux Distribution for Equilibrium Core	44
Figure 13	Thermal Flux Distribution for Batch Core	45
Figure 14	Thermal Flux Distribution for Equilibrium Core	46

Page

LIST OF TABLES

Table 1A	UAl_x Fuel Core Swelling Data	3
Table 1B	U_3O_8 Fuel Core Swelling Data	6
Table 2A	UAl_x Fuel Core Blister Data	8
Table 2B	U_3O_8 Fuel Core Blister Data	11
Table 3A	Training, Research, and Test Reactor Operating Parameters	14
Table 3B	Ford Nuclear Reactor Operating Parameters	14A
Table 4	Comparison of LEOPARD and HAMMER Results for MTR-Type Fuel	18
Table 5	Experimental and Calculated Results for Several Reactor Configurations	22
Table 6	Regular Fuel Element Shuffling Scheme	32
Table 7	Control Rod Fuel Element Shuffling Scheme	33
Table 8	Comparison of the Equilibrium Core Parameters with the Actual FNR Parameters	35
Table 9	Core Physics Parameters for Equilibrium Core	37
Table 10	Core Physics Parameters for Batch Core	38

REFERENCES 49

BIBLIOGRAPHY 51

1. INTRODUCTION

As part of the national plan for development of high uranium density research and test reactor fuel to accomodate the use of low enrichment uranium (LEU) fuel, the Ford Nuclear Reactor (FNR) proposes to test the use of 19.5 wt% enriched uranium fuel in the form of uranium aluminide (UAl_x) or uranium oxide (U_3O_8) in place of the present 93 wt% uranium aluminide fuel.

The use of less than 20% enrichment fuel gives the potential benefit of reducing the probability of uranium-235 diversion. An additional benefit is a possible reduction in the cost of security requirements for both fuel fabrication and fuel handling and storage.

This report includes information on fuel which is physically similar to the proposed LEU fuel and which has been satisfactorily tested under operating conditions similar to those of the Ford Nuclear Reactor.

Core physics calculations indicate that utilization of LEU fuel in the FNR core will result in a decrease in thermal flux of 12-20% in the core region and a decrease of 6-10% in the reflector region.

2. FUEL DESCRIPTION

The proposed LEU fuel meat is to be intermetallic uranium aluminide (UAL_3, UAL_4, UAL_2) or uranium oxide (U_3O_8) cermet, both of which are licensed for use by the FNR, clad in 6061 aluminum.

Fuel element overall dimensions and internal dimensions will remain identical to the dimensions of fuel presently being used in the FNR at two megawatts. Plate thickness will be 0.060 inches. The meat will be 0.030 inches and cladding 0.015 inches. Two plate thicknesses are presently in use at the FNR. Uranium-aluminum alloy fuel plates are 0.060 inches thick with 0.020 clad-0.020 meat-0.020 clad. Aluminide fuel plates are 0.050 inches thick with 0.015 clad-0.020 meat-0.015 clad. The FNR has operating experience with fuel plates which are 0.060 inches thick and which have 0.015 inch clad, and no problems have arisen.

The proposed meat thickness of 0.030 inches is dictated by an attempt to provide fuel with the same reactivity as present FNR fuel while reducing the enrichment from 93% to just under 20%. In order to provide the proper uranium-235 loading, the weight percent of the fissile compound in the fuel meat must be increased from the present 19.1 weight percent UAL_x or 16.8 weight percent U_3O_8 to approximately 56.5 weight percent UAL_x or 49.6 weight percent U_3O_8. Present uranium loading is 14.2 weight percent; the proposed loading is 42.0 weight percent.

3. OPERATING CONDITIONS

Fuel swelling data and fuel blister data, which were obtained for fuel plates made of materials similar to those in the FNR and which were determined at fuel temperature, pressure, and pH conditions similar to FNR conditions, were extracted from the data contained in reports referenced in the Safety Analysis bibliography and are tabulated in TABLE 1 and TABLE 2. All available data points are included.

The aluminum powder used in the proposed FNR fuel and in the test cores is a blend of nearly pure aluminum. 1100 aluminum is pure aluminum. The various powder blends (PB-01, PB-04, PB-32, PB-36) are essentially pure aluminum of specific grain sizes. 5214 is spherical aluminum powder with .05% iron and a total of .08% iron plus silicon permitted. X8001 is a nickel alloy of aluminum which is only slightly harder than 1100.

4. FUEL SWELLING

Table 1A provides UAL_x fuel swelling data.[1, 2, 3, 4, 5] Table 1B contains U_3O_8 fuel swelling data.[4] Test temperatures are as close as possible to the FNR peak operating temperature of 172°F. All test data were obtained at significantly higher pressures. Figure 1 is a plot of the UAL_x and U_3O_8 data points. Also shown on Figure 1 is the FNR fission density limit of 15×10^{20} fissions/cc and the calculated swelling rate for 100% dense fuels.

With the exception of one data point, the measured swelling rate is below the calculated swelling rate. It is expected that the measured swelling rate would be less than calculated because some voids are expected in core compacts and voids generally tend to reduce swelling.

No fuel failures were observed for the fission density-fuel swelling combinations plotted on Figure 1. Therefore, all of the available fuel swelling data at operating conditions similar to those in the FNR indicate that UAL_x and U_3O_8 fuel can be safely used in the FNR without failure due to swelling and that no reduction in the safety margin is expected.

5. FUEL BLISTERING

Table 2A provides UAL_x fuel blister data.[1, 2, 3, 5, 7] Table 2B contains U_3O_8 fuel blister data.[1, 8] Figure 2, a plot of fuel blister temperature versus fission density for the Table 2A and 2B data, shows that all blister failures occurred in fuel being operated at temperatures well above the FNR peak operating temperature of 172°F.

TABLE 1A

UAL_x FUEL CORE SWELLING DATA

Reactor	Fuel Characteristics									
Sample ID	Clad	Core	Weight Percent UAL_x	Weight Percent U	Core Temp, °F (°C)	Operating Pressure PSIG	pH	Fission Density f/cc X 10^{20}	Volume Change % Δ V/V	Ref
FNR	6061	5214	19.1	14.2	172 (78)	9.2	5-7	15.0		
MTR										
113-1	6061	6061	46.7	34.7	239 (115)	50	5-7	7.5	7.5	1
113-2	6061	6061	46.7	34.7	239 (115)	50	5-7	10.1	6.8	1
113-3	6061	6061	46.7	34.7	239 (115)	50	5-7	9.4	6.2	1
113-4	6061	6061	46.7	34.7	239 (115)	50	5-7	9.8	3.7	1
113-5	6061	6061	46.7	34.7	239 (115)	50	5-7	13.5	7.3	1
113-6	6061	6061	46.7	34.7	239 (115)	50	5-7	14.1	7.3	1
113-7	6061	6061	46.7	34.7	239 (115)	50	5-7	14.5	5.5	1
ETR										
I-1-1095	6061	X8001	51.0	37.9	230 (110)	200	5-7	6.9	0.8	2
I-1-1097	6061	X8001	51.0	37.9	230 (110)	200	5-7	5.6	0.8	2
I-12-727	APM786	X8001	51.0	37.9	230 (110)	200	5-7	10.9	3.9	2
I-1-584	6061	X8001	51.0	37.9	302 (150)	200	5-7	7.2	0.6	2
I-69-1579	6061	MD101	60.0	44.6	302 (150)	200	5-7	16.5	3.6	2
I-71-1594	6061	MD101	77.0	57.2	302 (150)	200	5-7	24.7	1.1	2
I-69-1580	6061	MD101	60.0	44.6	338 (170)	200	5-7	9.4	1.8	2
I-70-1583	6061	MD101	65.0	48.3	338 (170)	200	5-7	11.0	1.2	2
I-70-1584	6061	MD101	65.0	48.3	338 (170)	200	5-7	16.2	4.9	2

TABLE 1A

UAL_x FUEL CORE SWELLING DATA

Reactor	Fuel Characteristics									
Sample ID	Clad	Core	Weight Percent UAL_x	Weight Percent U	Core Temp, °F (°C)	Operating Pressure PSIG	pH	Fission Density f/cc X 10^{20}	Volume Change % ΔV/V	Ref
FNR	6061	5214	19.1	14.2	172 (78)	9.2	5-7	15.0		
ETR										
169-4	6061	X8001	61.9	46.0	228 (109)	200	5-7	26.3	2.0	3
169-5	6061	X8001	61.9	46.0	228 (109)	200	5-7	28.8	4.7	3
169-11	6061	X8001	52.0	38.7	228 (109)	200	5-7	23.1	4.7	3
169-12	6061	X8001	52.0	38.7	228 (109)	200	5-7	24.3	5.9	3
169-19	6061	X8001	43.0	32.0	228 (109)	200	5-7	19.7	4.7	3
169-36	6061	X8001	52.8	39.2	228 (109)	200	5-7	25.1	6.4	3
169-37	6061	X8001	52.7	39.2	228 (109)	200	5-7	25.5	6.0	3
169-38	6061	X8001	52.7	39.2	228 (109)	200	5-7	25.0	7.4	3
169-39	6061	X8001	52.7	39.2	228 (109)	200	5-7	23.9	5.7	3
HFIR										
32-4	6061	PB-32*	51.0	37.9	176 (80)	1000	5-7	17.9	8.8	4
34-2	6061	PB-36	53.0	39.4	190 (88)	1000	5-7	19.5	6.8	4
14-3	6061	PB-32	53.0	39.4	198 (92)	1000	5-7	20.2	7.4	4
15-4	6061	PB-32	63.0	46.8	208 (98)	1000	5-7	22.2	6.1	4
35-4	6061	PB-36	63.0	46.8	201 (94)	1000	5-7	21.4	4.8	4
25-4	6061	PB-32	64.0	47.6	205 (96)	1000	5-7	21.7	4.1	4

* Aluminum Powder Blends

TABLE 1A

UAL_x FUEL CORE SWELLING DATA

Reactor Sample ID	Fuel Characteristics: Clad	Core	Weight Percent UAL_x	Weight Percent U	Core Temp, °F (°C)	Operating Pressure PSIG	pH	Fission Density f/cc X 10^{20}	Volume Change % Δ V/V	Ref
FNR	6061	5214	19.1	14.2	172 (78)	9.2	5-7	15.0		
FR2 (Kalsruhe, Germany)										
1-4	1100	1100	50	37.1	158 (70)	50	5-7	5.8	2.0	5
2-4	1100	1100	50	37.1	158 (70)	50	5-7	16.9	4.5	5
3-4	1100	1100	50	37.1	158 (70)	50	5-7	12.2	4.0	5
4-1	1100	1100	50	37.1	158 (70)	50	5-7	9.4	3.5	5
5-3	1100	1100	45.5	33.8	158 (70)	50	5-7	9.4	3.5	5
6-4	1100	1100	45.5	33.8	158 (70)	50	5-7	7.6	4.0	5
7-2	1100	1100	50	37.1	158 (70)	50	5-7	15.8	5.0	5
8-2	1100	1100	45.5	33.8	158 (70)	50	5-7	15.8	4.0	5

TABLE 1B

U_3O_8 FUEL CORE SWELLING DATA

Reactor	Fuel Characteristics									
Sample ID	Clad	Core	Weight Percent U_3O_8	Weight Percent U	Core Temp, °F (°C)	Operating Pressure PSIG	pH	Fission Density f/cc X 10^{20}	Volume Change % ΔV/V	Ref
FNR	6061	5214	16.8	14.2	172 (78)	9.2	5-7	15.0		
HFIR										
12-3	6061	PB-01*	47	39.7	192 (89)	1000	5-7	19.8	3.0	4
13-4	6061	PB-01	40	33.8	183 (84)	1000	5-7	18.1	3.8	4
22-4	6061	PB-04	50	42.3	187 (86)	1000	5-7	19.7	2.9	4
23-1	6061	PB-04	42	35.5	181 (83)	1000	5-7	18.1	3.1	4
ETR										
67-974	6061	PB-01*	40	33.8	401 (205)	200	5-7	17.9	4.7	4
67-982	6061	PB-01	40	33.8	383 (195)	200	5-7	18.0	5.1	4
67-986	6061	PB-01	40	33.8	392 (200)	200	5-7	18.1	6.2	4
56-899	6061	PB-01	50	42.3	302 (150)	200	5-7	11.7	1.4	4
56-957	6061	PB-01	50	42.3	302 (150)	200	5-7	22.4	7.6	4
3-893	6061	PB-04	45	38.0	347 (175)	200	5-7	15.5	2.0	4
68-997	6061	PB-04	49	41.4	347 (175)	200	5-7	19.7	3.6	4
68-1638	6061	PB-04	49	41.4	428 (220)	200	5-7	12.7	0.4	4
68-1633	6061	PB-04	49	41.4	419 (215)	200	5-7	12.7	0.4	4
68-1642	6061	PB-04	49	41.4	410 (210)	200	5-7	12.7	1.7	4
68-1605	6061	PB-04	49	41.4	329 (165)	200	5-7	19.9	3.0	4
68-1607	6061	PB-04	49	41.4	338 (170)	200	5-7	19.5	3.1	4

* Aluminum Powder Blends

FIGURE 1

FUEL CORE SWELLING

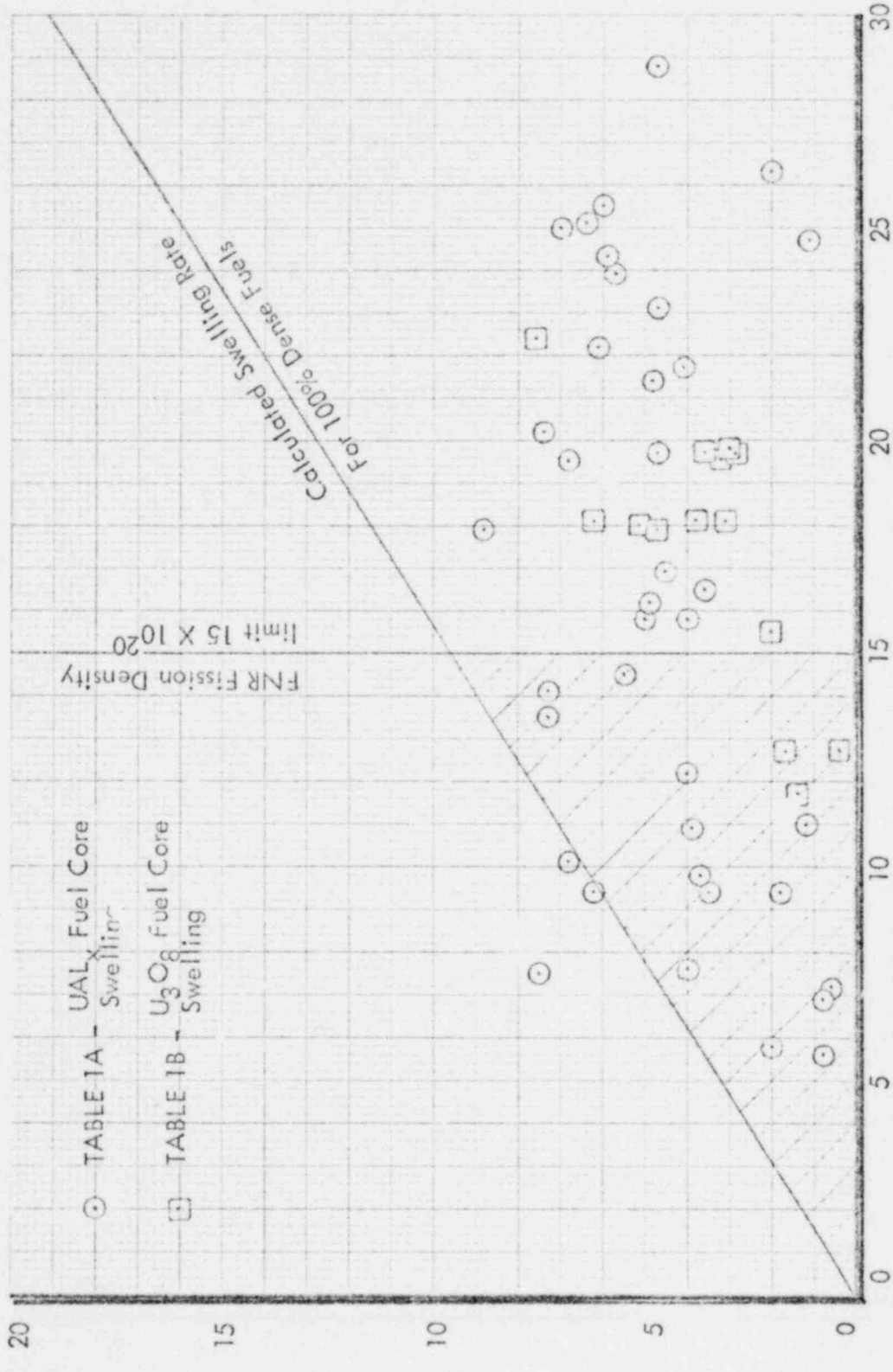

TABLE 2A

UAL_x FUEL CORE BLISTER DATA

Reactor	Fuel Characteristics									
			Weight Percent							
Sample ID	Clad	Core	UAL_x	U	Core Temp, °F (°C)	Operating Pressure PSIG	pH	Fission Density $f/cc \times 10^{20}$	Blister Temp, °F (°C)	Ref
FNR	6061	5214	19.1	14.2	172 (78)	9.2	5-7	15.0		
ETR										
E-107	6061	X8001	54.0	40.1	403 (206)	200	5-7	10.4	1094 (590)	7
E-508	6061	X8001	54.0	40.1	403 (206)	200	5-7	10.7	1094 (590)	7
E-510	6061	X8001	54.0	40.1	403 (206)	200	5-7	11.0	1094 (590)	7
E-507	6061	X8001	54.0	40.1	403 (206)	200	5-7	11.2	1094 (590)	7
I-1-1095	6061	X8001	51.0	37.9	230 (110)	200	5-7	6.9	1004 (540)	2
I-1-1097	6061	X8001	51.0	37.9	230 (110)	200	5-7	5.6	1004 (540)	2
I-12-727	APM786	X8001	51.0	37.9	230 (110)	200	5-7	10.9	1004 (540)	2
I-69-1579	6061	MD101	60.0	44.6	302 (150)	200	5-7	7.2	1112 (600)	2
I-71-1594	6061	MD101	77.0	57.2	302 (150)	200	5-7	24.7	806 (430)	2
I-69-1580	6061	MD101	60.0	44.6	338 (170)	200	5-7	9.4	1112 (600)	2
I-70-1583	6061	MD101	65.0	48.3	338 (170)	200	5-7	11.0	1112 (600)	2
I-70-1584	6061	MD101	65.0	48.3	338 (170)	200	5-7	16.2	1112 (600)	2
I-71-1593	6061	MD101	77.0	57.2	338 (170)	200	5-7	12.6	1112 (600)	2
169-4	6061	X8001	61.9	46.0	228 (109)	200	5-7	26.3	1050 (565)	3
169-5	6061	X8001	61.9	46.0	228 (109)	200	5-7	28.8	> 1050 (> 565)	3
169-11	6061	X8001	52.0	38.7	228 (109)	200	5-7	23.1	1000 (538)	3
169-12	6061	X8001	52.0	38.7	228 (109)	200	5-7	24.3	1050 (565)	3
169-19	6061	X8001	43.0	32.0	228 (109)	200	5-7	19.7	1050 (565)	3
169-36	6061	X8001	52.8	39.2	228 (109)	200	5-7	25.1	> 1050 (> 565)	3
169-37	6061	X8001	52.7	39.2	228 (109)	200	5-7	25.5	1000 (538)	3
169-38	6061	X8001	52.7	39.2	228 (109)	200	5-7	25.0	1000 (538)	3
169-39	6061	X8001	52.7	39.2	228 (109)	200	5-7	23.9	1050 (565)	3

TABLE 2A

UAL_x FUEL CORE BLISTER DATA

Reactor / Sample ID	Fuel Characteristics: Clad	Core	Weight Percent UAL_x	Weight Percent U	Core Temp, °F (°C)	Operating Pressure PSIG	pH	Fission Density f/cc X 10^{20}	Blister Temp, °F (°C)	Ref
FNR	6061	5214	19.1	14.2	172 (78)	9.2	5-7	15.0		
MTR										
113-8	6061	6061	46.7	34.7	239 (115)	50	5-7	4.5	> 1100 (> 594)	1
113-9	6061	6061	46.7	34.7	239 (115)	50	5-7	5.7	> 1100 (> 594)	1
113-10	6061	6061	46.7	34.7	239 (115)	50	5-7	6.2	> 1100 (> 594)	1
113-11	6061	6061	46.7	34.7	239 (115)	50	5-7	7.2	> 1100 (> 594)	1
113-12	6061	6061	46.7	34.7	239 (115)	50	5-7	10.5	> 1100 (> 594)	1
113-13	6061	6061	46.7	34.7	239 (115)	50	5-7	9.2	1022 (550)	1
113-14	6061	6061	46.7	34.7	239 (115)	50	5-7	9.5	932 (500)	1
113-15	6061	6061	46.7	34.7	239 (115)	50	5-7	11.3	932 (500)	1
113-16	6061	6061	46.7	34.7	239 (115)	50	5-7	12.5	1067 (575)	1
113-17	6061	6061	46.7	34.7	239 (115)	50	5-7	20.3	932 (500)	1
FR2 (Kalsruhe, Germany)										
1-4	1100	1100	50	37.2	158 (70)	50	5-7	5.8	> 932 (> 500)	5
2-4	1100	1100	50	37.2	158 (70)	50	5-7	16.9	> 932 (> 500)	5
3-4	1100	1100	50	37.2	158 (70)	50	5-7	12.2	> 932 (> 500)	5
4-1	1100	1100	50	37.2	158 (70)	50	5-7	9.4	> 932 (> 500)	5
5-3	1100	1100	45.5	33.8	158 (70)	50	5-7	9.4	> 932 (> 500)	5
6-4	1100	1100	45.5	33.8	158 (70)	50	5-7	7.6	> 932 (> 500)	5
7-2	1100	1100	50	37.2	158 (70)	50	5-7	15.8	> 932 (> 500)	5
8-2	1100	1100	45.5	33.8	158 (70)	50	5-7	15.8	> 932 (> 500)	5
9-3	1100	1100	50	37.2	158 (70)	50	5-7	5.8	> 932 (> 500)	5
10-1	1100	1100	45.5	33.8	158 (70)	50	5-7	5.8	> 932 (> 500)	5
11-4	1100	1100	50	37.2	248 (120)	50	5-7	10.0	> 932 (> 500)	5
12-4	1100	1100	50	37.2	275 (135)	50	5-7	10.0	> 932 (> 500)	5

TABLE 2A

UAL_x FUEL CORE BLISTER DATA

Reactor	Fuel Characteristics									
			Weight Percent							
Sample ID	Clad	Core	UAL_x	U	Core Temp, °F (°C)	Operating Pressure PSIG	pH	Fission Density f/cc X 10^{20}	Blister Temp, °F (°C)	Ref
FNR	6061	5214	19.1	14.2	172 (78)	9.2	5-7	15.0		
FR2 (Kalsruhe, Germany)										
13-2	1100	1100	50	37.2	302 (150)	50	5-7	10.0	> 932 (> 500)	5
14-2	1100	1100	50	37.2	302 (150)	50	5-7	19.0	> 932 (> 500)	5
15-2	1100	1100	45.5	33.8	302 (150)	50	5-7	19.0	> 932 (> 500)	5
16-2	1100	1100	50	37.2	302 (150)	50	5-7	25.9	> 932 (> 500)	5
17-2	1100	1100	45.5	33.8	302 (150)	50	5-7	25.9	> 932 (> 500)	5
18-1	1100	1100	50	37.2	302 (150)	50	5-7	21.6	> 932 (> 500)	5
19-1	1100	1100	45.5	33.8	302 (150)	50	5-7	21.6	> 932 (> 500)	5
20-2	1100	1100	45.5	33.8	302 (150)	50	5-7	21.6	> 932 (> 500)	5

TABLE 2B

U_3O_8 FUEL CORE BLISTER DATA

Reactor	Fuel Characteristics									
			Weight Percent							
Sample ID	Clad	Core	U_3O_8	U	Core Temp, °F (°C)	Operating Pressure PSIG	pH	Fission Density f/cc X 10^{20}	Blister Temp, °F (°C)	Ref
FNR	6061	5214	16.8	14.2	172 (78)	9.2	5-7	15.0		
MTR										
1	6061	X8001	----	----	239 (115)	50	5-7	2.5	716 (380)	1
2	6061	X8001	----	----	239 (115)	50	5-7	5.0	716 (380)	1
3	6061	X8001	----	----	239 (115)	50	5-7	5.0	824 (440)	1
4	6061	X8001	----	----	239 (115)	50	5-7	8.0	716 (380)	1
5	6061	X8001	----	----	239 (115)	50	5-7	8.2	824 (440)	1
6	6061	X8001	----	----	239 (115)	50	5-7	8.3	716 (380)	1
7	6061	X8001	----	----	239 (115)	50	5-7	10.5	716 (380)	1
ETR										
68-1633	6061	PB-04*	49	41.4	419 (215)	200	5-7	12.7	1022 (550)	8
68-1638	6061	PB-04	49	41.4	428 (220)	200	5-7	12.7	1022 (550)	8
68-1643	6061	PB-04	49	41.4	410 (210)	200	5-7	12.7	1022 (550)	8
68-997	6061	PB-04	49	41.4	347 (175)	200	5-7	19.7	932 (500)	8
68-1605	6061	PB-04	49	41.4	329 (165)	200	5-7	19.9	932 (500)	8
68-1607	6061	PB-04	49	41.4	338 (170)	200	5-7	19.5	932 (500)	8

* Aluminum Powder Blends

FIGURE 2

FUEL CORE BLISTER TEMPERATURES

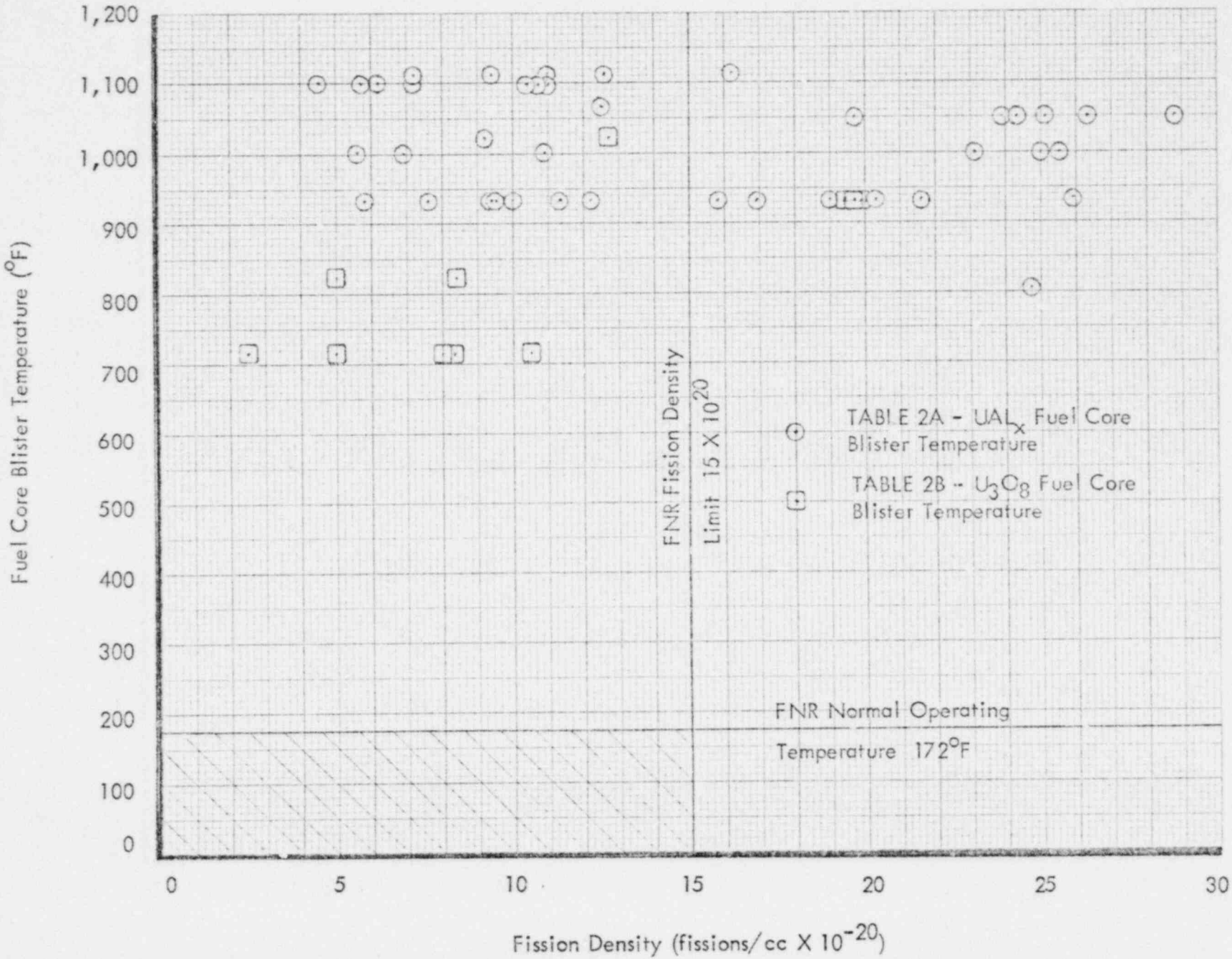

All of the available fuel blister data for UAL_x and U_3O_8 fuel which has been operated under conditions similar to those in the FNR indicate that UAL_x and U_3O_8 fuel can be safely used in the FNR without failure due to blistering and without reducing the safety margin.

6. FAILURE HISTORY

Table 3 provides a listing of reactor operating parameters for those reactors for which test data were provided in Table 1 and Table 2 and for the Ford Nuclear Reactor. Table 3 shows that the Advanced Test Reactor (ATR) routinely uses fuel with higher UAL_x loading than that proposed for FNR low enrichment uranium fuel. Similarly, the High Flux Isotope Reactor (HFIR) routinely uses fuel with U_3O_8 loadings equivalent to that proposed for the FNR.

The swelling and blistering data in Section 5 is for fuel cores with several aluminum alloys, but not 5214 alloy. The different core materials (powder blends, 1100, 6061, and X8001) show no significant effects on swelling and blistering characteristics. In addition, alloy 5214 is quite similar to 1100 as the list of constituents below indicates. Both essentially are pure aluminum powder.

	Constituents	1100	5214
Maximum:	Boron	---	0.001%
	Cadmium	---	0.002%
	Copper	0.20%	0.20%
	Iron	---	0.05%
	Lithium	---	0.008%
	Manganese	0.05%	
	Silicon + Iron	1.00%	0.25%
	Zinc	0.10%	0.10%
	Others	0.15%	---
Minimum:	Aluminum	99%	99.7%

The failure history for the Advanced Test Reactor in Section 6.1 provides extensive operational data. Advanced Test Reactor fuel cores are 5214 aluminum.

6.1 Uranium Aluminide (UAL_x)

To date, the Advanced Test Reactor has operated over 89,000 UAL_x fuel plates up to the depletion limit of 2.3×10^{21} fissions/cc. In all of these fuel plates, only one (and this one was found to have thinly rolled clad) allowed fission product leakage into the ATR coolant. The plate was operated to depletion.

The thin clad was attributed to "dogboning" in the fuel core which has been eliminated by sloping the edges of the core ingot before rolling.

To date, twenty-one 93% enrichment aluminide fuel plates with 5214 aluminum cores have been operated to partial depletion in the Ford Nuclear Reactor. The peak fission density among these elements is 1.27×10^{20} fissions/cc. Inspections for fuel damage are not specifically performed, but the plates have shown no evidence and given no indication of swelling, blistering, warping, or cracking.

TABLE 3A

TRAINING, RESEARCH, AND TEST REACTOR OPERATING PARAMETERS

Parameter	Materials Testing Reactor (MTR)[1, 23]	Engineering Test Reactor (ETR)[1, 23]	Advanced Test Reactor (ATR)[1, 23]	High Flux Isotope Reactor (HFIR)[9, 23]	High Flux Beam Reactor (HFBR)[10, 23]
Year placed in service	1952	1956	1967	1965	1965
Thermal power (MW)	40	175	40	100	40
Thermal power density (MW/l)	0.75	1.2	2.8	1.5	0.5
Fuel element meat volume (cc)	365	550	798	3475	870
U-235 per element (gm)	200	400	975	2600	315
U-235 burnup (%)	--	25	25	30.6	34
Peak fission density (fiss/cc)	---	1.8×10^{21}	2.3×10^{21}	1.9×10^{21}	1.24×10^{21}
Fuel element surface area (ft^2)	15	23	34	147	36
Heat flux (BTU/ft^2-hr)	3.5×10^5	5×10^5	4×10^5	2.5×10^5	3.8×10^5
Coolant flow rate (gpm)	24,000	44,000	16,000	17,000	16,6000
Fuel element materials:					
Cladding	1100 Al	1100 Al	6061 Al	6061 Al	6061 Al
Core	1100 Al	5214 Al	5214 Al	1100 Al	1100 Al
Core Fissile Compound (Weight %)	UAL_x 46.0	UAL_x 40.6	UAL_x 45.1 - 60.8	U_3O_8 25.6	U_3O_8 40.6
Core Uranium (Weight %)	34.2	30.2	33.5 - 45.2	21.6	34.3
Fuel Plate thickness (in)					
Clad	0.015	0.015	0.015	0.010	0.014
Core	0.020	0.020	0.020	0.030	0.023
Overall	0.050	0.050	0.050	0.050	0.051

TABLE 3B

FORD NUCLEAR REACTOR OPERATING PARAMETERS

Parameter	High Enrichment Fuel		Proposed Low Enrichment Fuel	
	Uranium Aluminum Alloy (U-Al)	Uranium Aluminide (UAl_x)	Uranium Aluminide (UAl_x)	Uranium Oxide (U_3O_8)
Year placed in service	1958	1978	1980	Undetermined
Thermal power (MW)	2	2	2	2
Thermal power density (MW/l)	.025	.025	.025	.025
Fuel element meat volume (cc)	354	335	502	502
U-235 per element (gm)	140	140	167	167
U-235 burnup (%)	35	35	50	50
Peak fission density (fiss/cc)	1.5×10^{20}	1.5×10^{20}	2.6×10^{20}	2.6×10^{20}
Fuel element surface area (ft^2)	15	15	15	15
Heat flux (BTU/ft^2-hr)	3.68×10^4	3.68×10^4	3.68×10^4	3.68×10^4
Coolant flow rate (gpm)	980	980	980	980
Fuel element materials:				
Cladding	6061 Al	6061 Al	6061 Al	6061 Al
Core	1100 Al	5214 Al	5214 Al	1100 Al
Core Fissile Compound (Weight %)	Not Applicable	19.1	56.5	49.6
Core Uranium (Weight %)	14.2	14.2	42.0	42.0
Fuel plate thickness (in)				
Clad	.020	.015	.015	.015
Core	.020	.020	.030	.030
Overall	.060	.050	.060	.060
Coolant flow channel thickness (in)	.117	.125	.117	.117

6.2 Uranium Oxide (U_3O_8)

To date, the High Flux Isotope Reactor has operated over 76,000 U_3O_8 fuel plates up to the depletion limit 1.9×10^{21} fissions/cc with no failures. On two occasions, fuel plates developed suspected fission product leaks. In one case, the apparent leak was so insignificant that the element was operated to depletion.[9] In the second case, the element was removed after 1500 MWD. Destructive tests showed no evidence of blisters, cladding separation, matrix cracking, or any defects indicative of incipient failure.

7. FUEL SPECIFICATIONS

7.1 Uranium Aluminide (UAL_x)

FNR fuel specifications have been developed in co-operation with the ATR staff at the Idaho National Engineering Laboratory and Atomics International (AI), the ATR fuel manufacturer. The UAL_x specification is identical to that specified by ATR. The present ATR fission density limit is 23×10^{20} fissions/cc.

The fuel swelling and bl. er data in the references and tables often refer to aluminide as UAL_3. The early intermetallic fuel development work in Idaho was for the fabrication and testing of UAL_3 material and so the early designation was UAL_3. During this early fuel testing work, it was recognized that aluminide was not purely UAL_3. In 1966, UAL_3 was identified as the major crystalline component with UAL_2 and UAL_4 present.[11] Current ATR fuel powder specifications require the UAL_3 content to be at least 50%.

The FNR fuel powder specification calls for uranium aluminide powder containing at least 50% UAL_3.

7.2 Uranium Oxide (U_3O_8)

U_3O_8 fuel specifications will be developed in co-operation with Oak Ridge National Laboratory (ORNL) and Brookhaven National Laboratory (BNL) should U_3O_8 fuel be used in the FNR.

8. HEAT TRANSFER CHARACTERISTICS

The proposed LEU fuel heat transfer characteristics will be essentially identical to those of alloy fuel which has been used in the FNR core since 1957 and still comprises the majority of the fuel elements in the core. Overall element dimensions. fuel plate dimensions, and coolant flow channel width and thickness are unchanged.

Peak fuel temperature in the hottest FNR fuel plate is calculated to be 172°F. The margin of operational safety will not be changed by the use of LEU fuel.

9. CORE PHYSICS

The core physics analysis of the proposed LEU fuel reflects two basic differences from the HEU fuel currently used in the FNR core: (1) the fuel loading will be increased from 140 grams to 167.3 grams of ^{235}U per 18-plate element to compensate for increased neutron absorption in ^{238}U and spectrum hardening, and (2) the fuel meat thickness will be increased from .020 inches to .030 inches, with clad thickness decreased from .020 to .015 inches, to maintain the same total fuel plate thickness while allowing for the larger amount of ^{238}U. The proposed LEU fuel specifications are selected so that the excess reactivity of a batch fresh core configuration is the same for both the current HEU fuel and the proposed LEU fuel.

The core physics analysis includes examination of the effect of LEU fuel on core power distribution, in-core and ex-core flux distribution, cycle length and operating characteristics, core excess reactivity and shutdown margin.

9.1 Description of Calculational Methods

9.1.1 Computer Codes Used for Core Physics Analysis

All analysis was performed with the standard, well-verified production codes LEOPARD[12], EPRI-HAMMER[13], 2DB[14], ANISN[15], TWOTRAN[16], and VENTURE[17]. Brief descriptions of code capabilities are:

1) LEOPARD - a zero-dimensional unit-cell code using the MUFT/SOFOCATE scheme (54 fast and 172 thermal groups); has depletion capability; cross-section library consists of an early industrial data set.

2) EPRI-HAMMER - a one-dimensional integral transport theory code using 54 fast and 30 thermal groups; cross-section library constructed from ENDF/B-IV data.

3) 2DB - a two-dimensional multi-group diffusion theory code with depletion capability.

4) ANISN - a one-dimensional discrete ordinates transport theory code.

5) TWOTRAN-II - a two-dimensional discrete ordinates transport theory code.

6) VENTURE - a three-dimensional multi-group diffusion theory code

9.1.2 Code Modifications

The LEOPARD code originally performed a spectrum calculation for lattices consisting of cylindrical fuel rods. The code was modified

to allow slab geometry and separate few-group edits for both lattice and non-lattice regions. The principal modification was in the calculation of thermal disadvantage factors by the ABH method for slab geometry[18].

The modified LEOPARD code compares satisfactorily with the EPRI-HAMMER code, an accurate, well-verified code used in the analysis of benchmark critical experiments.[19] A typical comparison of k_∞ and two-group parameters in Table 4 shows that despite the many engineering approximations in the LEOPARD code, it compares quite well with the more accurate HAMMER code. Differences in few-group constants are due primarily to differences in the cross-section libraries - HAMMER uses ENDF/B-IV data while LEOPARD uses an early industrial data set.

The 2DB code has been modified to allow a macroscopic depletion capability via interpolation of macroscopic cross sections as a function of depletion. In addition, the isotopic balance equations for xenon and iodine have been included to allow the correct xenon levels within the core as a function of position and time (and macroscopic absorption cross sections are appropriately modified). Other modifications to 2DB have been aimed at automating data handling (e.g., the link with LEOPARD to produce macroscopic cross sections as a function of depletion) and improving fuel shuffling and edit capabilities.

9.1.3 Basic Calculation Method

The LEOPARD and 2DB codes were used for routine calculations of core reactivity, depletion effects, and power and flux distributions. Special methods for control rods and core leakage flux are described in subsequent sections. For both HEU and the proposed LEU fuel, the following scheme was followed:

1) The LEOPARD code was used to generate few-group cross sections. For most applications, two energy groups (fast and thermal) were used, although four energy groups were chosen for several detailed calculations.

   The geometry chosen was a unit cell in slab geometry consisting of a lattice region and a non-lattice or extra region. The lattice region was composed of fuel meat, clad and water channel. For regular assemblies, the extra region consisted of the side plates, non-active portions of fuel plates, and inter-assembly water gaps, which were homogenized on a volume basis. For special* fuel assemblies, the central water hole was also included in the extra region.

   Few-group macroscopic cross-section sets were generated as functions of depletion for the lattice and non-lattice regions and the total assembly.

   For the water reflector and heavy water tank, the extra region was chosen as H_2O or D_2O with a .25% H_2O content with a volume fraction

*Special is used in this section to designate control assemblies.

Table 4. Comparison of LEOPARD and HAMMER Results for MTR-type Fuel

	93% Alloy		19.5% UAl_x	
	LEOPARD	HAMMER	LEOPARD	HAMMER
k_∞	1.5477	1.5500	1.5150	1.5116
ϕ_1/ϕ_2	2.41	2.40	2.76	2.75
Age	51.5	49.9	49.1	47.5
D_1	1.434	1.372	1.424	1.360
Σ_{a1}	0.00204	0.00182	0.00358	0.00344
Σ_{r1}	0.0258	0.0257	0.0254	0.0253
$\nu\Sigma_{f1}$	0.00206	0.00223	0.00256	0.00274
D_2	0.284	0.272	0.280	0.269
Σ_{a2}	0.0597	0.0594	0.0676	0.0668
$\nu\Sigma_{f2}$	0.0948	0.0935	0.110	0.108

arbitrarily set equal to that of the lattice region. The extra region few-group cross sections obtained in this manner were used for the reflector and heavy water tank in the subsequent global calculation.

2) Global diffusion theory calculations were performed with the 2DB code. Three spatial mesh descriptions were used in x-y geometry: a homogeneous description, with a 2x2 mesh per assembly, was used for survey calculations, equilibrium core studies, and cycle length studies. A discrete representation, using a 6x6 mesh per assembly with the lattice and non-lattice portions of an assembly explicitly represented, was used for detailed analysis of power and flux distributions, temperature coefficient, and control rod reactivity worth. A discrete representation with a 12x12 mesh per assembly was used for verifying the adequacy of the 2x2 and 6x6 representations, and for comparison with the measured flux distributions.

   Depletion was accounted for on the assembly level by interpolating macroscopic cross sections as a function of depletion (MWD/MT) for the particular assembly in question. The fuel shuffling capability in the 2DB code allowed actual FNR operation to be simulated. The axial buckling term for the 2DB code used to approximate transverse leakage was based on the active core height with a reflector savings correction.

9.1.4 Control Rod Worth Calculations

FNR control (shim) rods are boron stainless steel containing 1.5 w/o natural boron. They are essentially black to thermal neutrons and cause a drastic thermal flux depression when inserted. The presence of such strong localized absorbers necessitates the use of transport theory codes to adequately describe the large flux gradients. However, in a small high leakage core like the FNR, control rod effects are not strictly local; therefore whole core calculations are needed, but are prohibitively expensive for transport theory codes. To accurately treat both local and global effects, transport theory codes were used for assembly level calculations to develop effective diffusion theory constants for global calculations. The method developed is a variation of the "NGD blackness method"[20] and has proved quite accurate.

Few-group constants for the control rod and surrounding water were obtained from the EPRI-HAMMER code for a cylindricized special assembly. Due to the strong spectral/spatial coupling in the rod it was necessary to obtain few-group cross sections for three control rod regions - a surface layer .1 cm thick, a second layer .3 cm thick, and the central region. Since few thermal neutrons reach the central region, the control rod perimeter, rather than volume, was preserved in the

geometric representation. Few-group constants for the special element lattice and side regions were obtained from the EPRI-HAMMER calculations for one half of a special element in slab geometry.

To accurately model the local effects of an inserted rod, the two-dimensional transport code TWOTRAN was used in fine-mesh calculations for a special assembly surrounded on all sides by one half of a regular assembly. Three regions of the rod and the surrounding water were explicitly represented, while the surrounding lattice regions were homogenized.

To develop effective few-group diffusion theory constants for use in global 2DB calculations, the 2DB code was used for the same geometry as in TWOTRAN calculations, except that the control rod and surrounding water were homogenized. Both fast and thermal absorption cross sections were varied until the 2DB calculation yielded the same relative absorption in the control region as the TWOTRAN result in each group. The resulting few-group constants for the control region were then used in global 2DB calculations. Although the flux distribution within the control region differs from the transport theory results, we believe the relative absorption in the control region and the flux in the surrounding fuel is accurately predicted in this scheme.

Control rod worth was then determined by comparing global 2DB calculations for the 6x6 mesh/assembly description with and without control rod inserted.

9.1.5 Calculational Methods for Temperature Coefficient of Reactivity and Xenon Reactivity Worth

Calculation of the temperature coefficient of reactivity and of reactivity worth of xenon poisoning was performed with global 2DB calculations with a 6x6 mesh/assembly description. The two-group cross sections for these 2DB cases were obtained from unit-cell calculations with the LEOPARD or the EPRI-HAMMER code, essentially following the basic scheme outlined in Section 9.1.3.

9.1.6 Equilibrium Core Model

Although the FNR core configuration and fuel shuffling pattern are, in practice, determined by operational requirements, an equilibrium core model was developed to allow for meaningful comparison of operating characteristics for the HEU and the proposed LEU cores. Our equilibrium core model essentially simulates a typical FNR shuffling pattern. Fresh fuel assemblies are placed near the control assemblies at the core center and are moved outward as they deplete. This pattern maximizes the control rod reactivity worth. The shuffling pattern was varied until the fuel depletion per cycle at each

assembly location obtained with global 2DB calculations closely matched that of the average FNR depletion at each location. The 2DB calculations performed over many cycles led to an equilibrium core model which, although not unique, is a realistic representation of the typical FNR operating cycle.

9.1.7 Ex-core Calculations

The ANISN and 2DB codes were used to calculate flux distributions in the H_2O and D_2O reflectors. Cross sections for the ANISN calculation were taken from the 100 group DLC-2 library and collapsed (with ANISN) to few groups. For 2DB calculations cross sections were generated by the LEOPARD code as explained in Section 9.1.3.

9.2 Comparison of Calculated and Experimental Results

The adequacy of the methods used for calculating core physics parameters for FNR core configurations has been established through comparing the calculated results with the data from several research and test reactors. In these verification efforts the calculated thermal flux and power distributions were compared with the experimental data obtained at the Bulk Shielding Reactor (BSR)[21], the High Flux Beam Reactor (HFBR)[22], and the FNR. The data for the BSR and HFBR cores were obtained at core configurations with MTR-type fuel elements similar to the FNR configurations.

9.2.1 Flux and Power Distributions

The measured thermal flux distributions and the core multiplication constants for the BSR loading 33 provide well documented experimental data[21] for a fresh critical core. The neutron flux distribution for this core was determined with x-y 2DB calculations utilizing a 6x6 and a 12x12 mesh per fuel assembly. Table 5 compares calculated and experimental results for the BSR and representative FNR configurations. Here the high neutron leakage causes the effective multiplication factor of the reactor to be sensitive to the input buckling value used to represent the leakage in the missing transverse direction. These calculations used an axial buckling of 2×10^{-3} cm^{-2}, which includes a calculated reflector savings.

Calculated results have been compared with the experimental data for a number of FNR core configurations. The assembly average power distribution in the Cycle 67 core was measured on March 17, 1971, with the core loading pattern presented in Figure 3. The power distribution was measured by thermocouples, with the coolant inlet temperature for each element measured inside the fuel element boxes and above the fuel plates, and the outlet temperature measured below the fuel plates in the element cone. From the assembly inlet

Case	Mesh/Group Structure	Core Reactivity		RMS Deviation[1] (thermal flux or assembly power)
		Measured	Calculated	
A (BSR #33)	6x6/2 group	1.006	1.009	11.3%[3]
	6x6/4 group	1.006	1.004	10.1%[3]
	12x12/2 group	1.006	1.012	7.8%[3]
B (FNR #67)	6x6/2 group	1.001	1.007[2]	9.3%[4]
C (FNR 1977 critical)	2x2/2 group	1.000	1.000[2]	---
	6x6/2 group	1.000	1.000[2]	---

Notes

1. RMS deviation = $\sqrt{\frac{1}{N-1}\sum_i \left(\frac{calc-exp}{exp}\right)_i^2}$

2. Corrected for measured xenon worth

3. Thermal flux deviation at 17 locations

4. Assembly power fraction deviation at 42 locations

Table 5. Experimental and Calculated Results for Several Reactor Configurations.

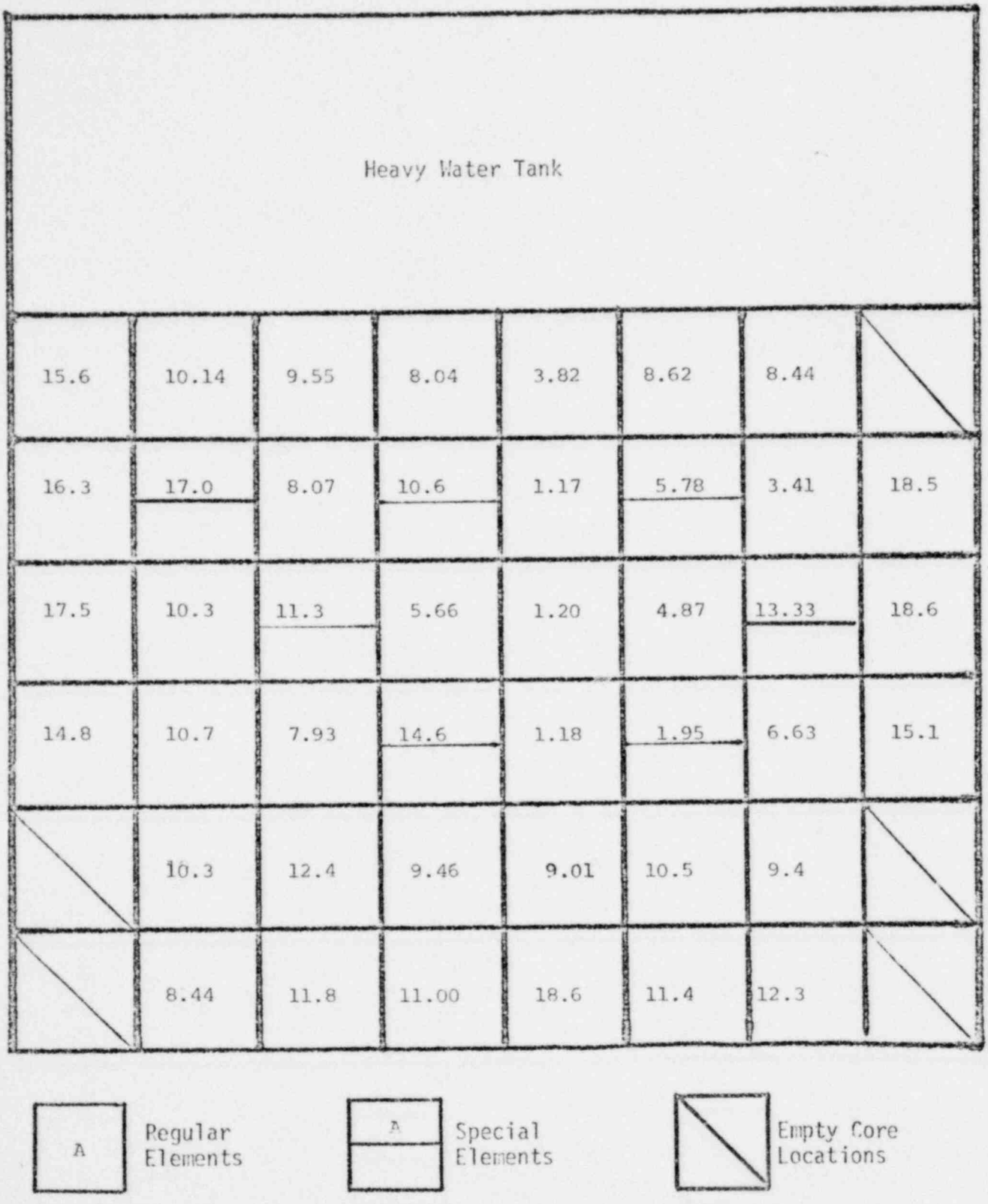

A: Assembly Burnup (MWD/assembly)

Figure 3. Fuel Burnup Distribution for FNR Cycle 67

and outlet temperatures, the power for each regular fuel element was calculated assuming equal coolant flow rate through each element. The assembly-average power distribution calculated by the 2DB code and the measured power distribution for the Cycle 67 core are presented in Figure 4. In this calculation the 2DB code predicted the core power distribution to within an rms deviation of 9.3%, as shown in Table 5.

The thermal flux distribution in the FNR Cycle 163B core was determined through flux maps obtained with a self-powered rhodium detector. The measurements were taken at the horizontal midplane of the core at the center of each regular fuel element. The core configuration for this cycle is shown in Figure 5, and a comparison of the calculated and measured thermal flux distributions is given in Figure 6. The calculated flux distribution shows good agreement with the measured distribution, with an rms deviation of 5.1%. Comparisons made for other fuel cycles show similar agreement between the measured and calculated results, with rms deviations in the range of 5 ~ 8%.

9.2.2 Ex-core Flux Distributions

Initial calculations to predict leakage neutron flux in the FNR D_2O tank concentrated on determining the accuracy of diffusion theory vs. transport theory calculations and on identifying critical parameters. Transport theory calculations performed in one-dimensional slab geometry with the ANISN code[15], and diffusion theory calculations performed with one- and two-dimensional codes were compared with experimental measurements for the FNR, BSR and HFBR. The results indicate that because of the large thermal diffusion length in D_2O, diffusion theory can accurately predict the thermal flux distribution for considerable distances into heavy water. The calculations for D_2O reflectors were sensitive to the transverse buckling due to the small D_2O macroscopic absorption cross-section. In a 2DB model of the HFBR with R-Z geometry, diffusion theory accurately simulated the thermal flux profile[22] at distances of .6-.8 meters into the D_2O reflector.

9.2.3 Control Rod Reactivity Worth

Control rod reactivity worth calculations were performed for the A, B, and C shim rods for FNR Cycle 67. The method for obtaining the rod worths was identical to that discussed in Sec. 9.1.4 except that the depletion of the fuel in the special fuel elements had to be accounted for. Accordingly, isotopic number densities for each of the special fuel element lattice regions were taken from a LEOPARD depletion calculation for a special element at the corresponding burnup points. These number densities were then used in place of BOL number densities, and the sequence of HAMMER calculations described in Sec. 9.1.4 was repeated. Full-core 6x6 2DB calculations were then

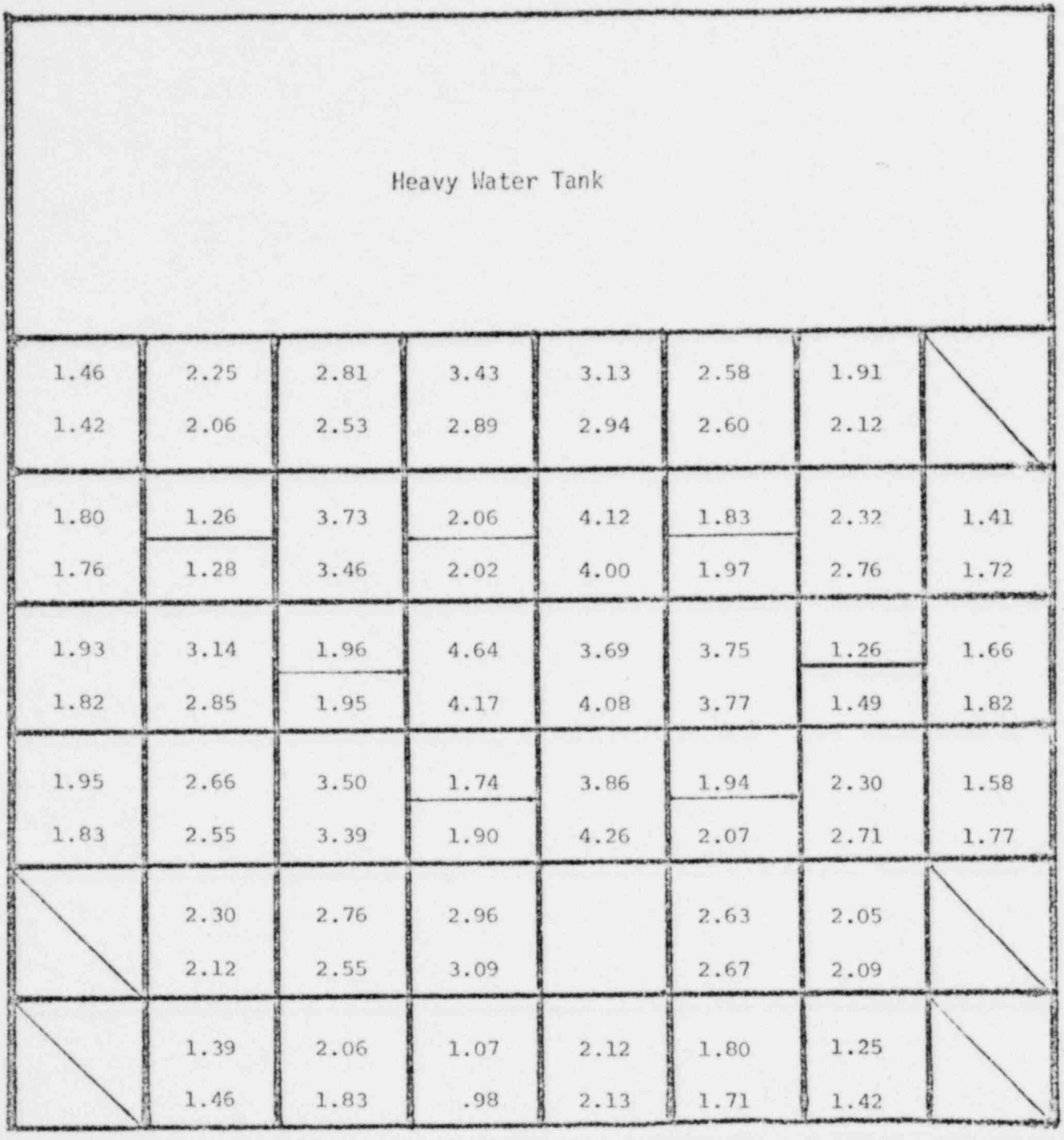

Figure 4. Experimental and Calculated Power Distributions for FNP Cycle 67

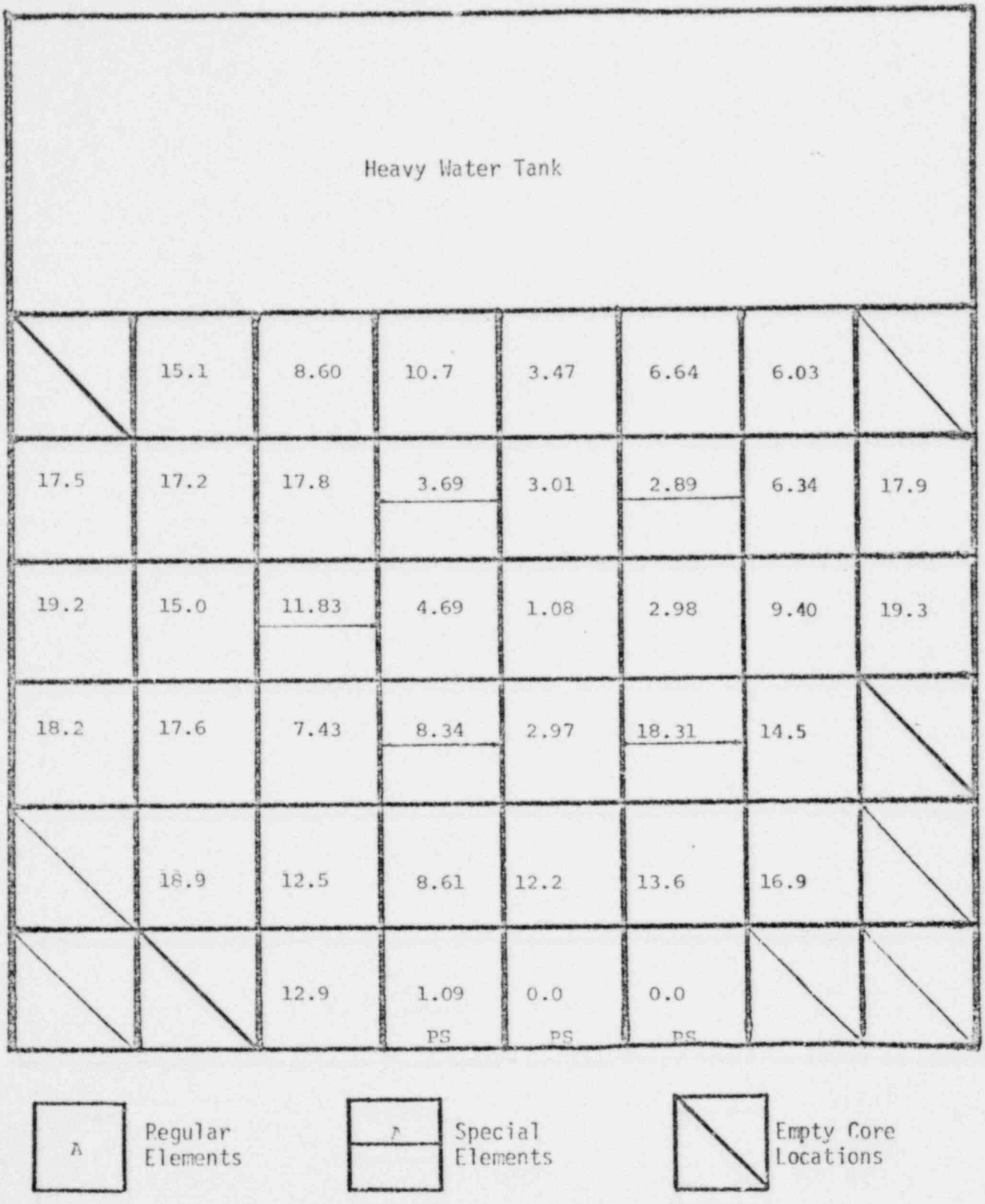

A: Assembly Burnup (MWD/assembly)
PS: Designates Pe[illegible] State Fuel Elements

Figure 5. Fuel Burnup Distribution for FNP Cycle 163B

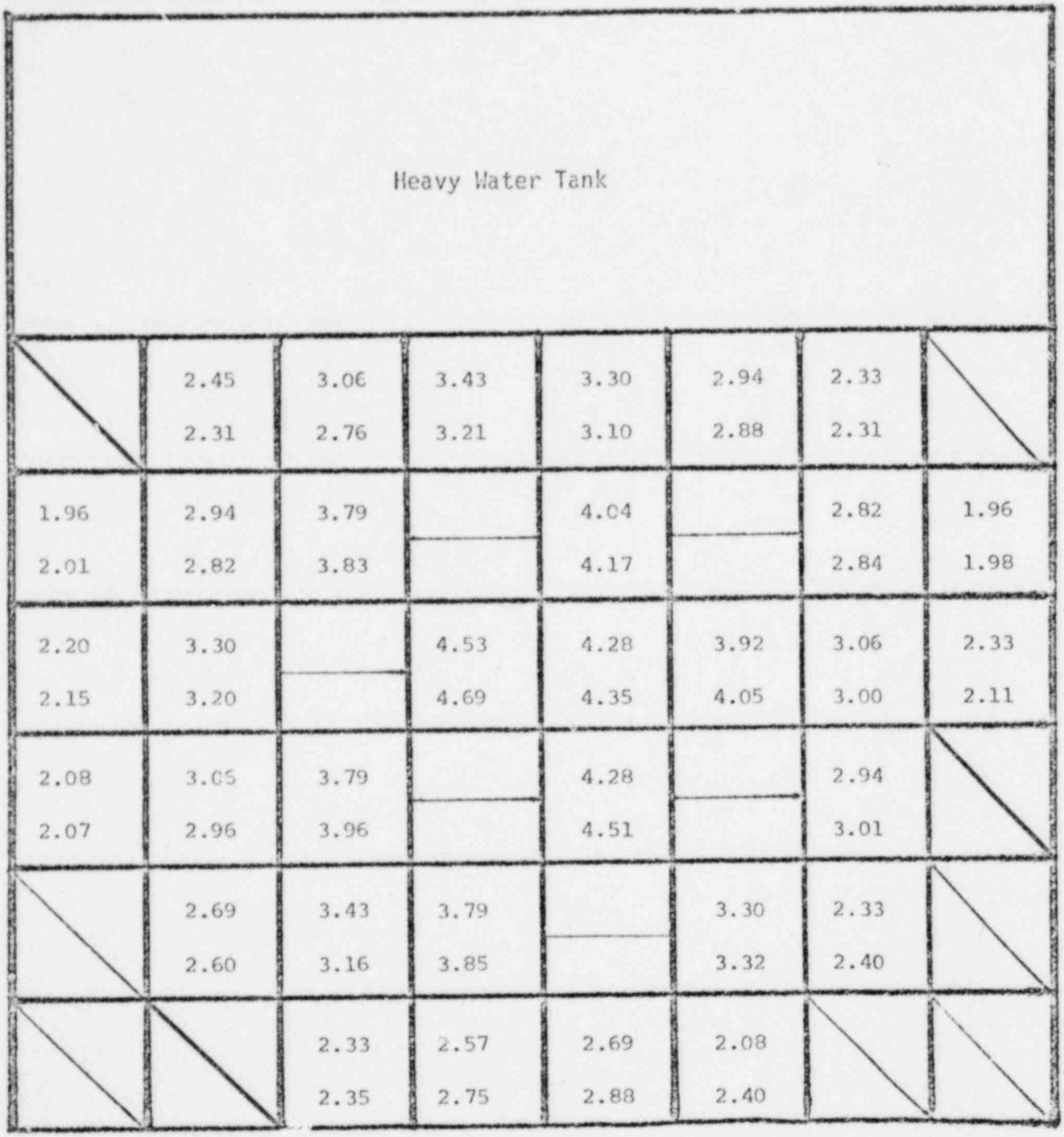

Figure 6. Experimental and Calculated Thermal Flux Distributions for FHR Cycle 163B

performed with all rods out and then separate runs were made with each of the three rods inserted. The calculated and measured rod worths compared as follows:

	Rod worth (% Δk/k)	
Shim rod	Measured	Calculated
A	2.22	2.20
B	2.11	2.11
C	1.72	1.73
Total rod worth	6.05	6.04

The agreement is excellent and provides verification of the methods for computing control rod worth in small, high-leakage cores. While there still exist some uncertainties in the actual measured rod worth, the close agreement indicates that the basic approach is valid.

9.3 Comparison of HEU and Proposed LEU Fueled Cores

To provide a meaningful and comprehensive comparison of HEU and proposed LEU fuels, it is necessary to account for both the intrinsic fuel properties and the FNR operating conditions. For the purpose of comparing core phyiscs parameters, two core configurations were analyzed for both fuels. The first configuration corresponds to a batch core consisting of fresh fuel assemblies, while the second configuration is based on an equilibrium core. The batch core configuration allows a comparison of undepleted HEU and LEU fuels, while the equilibrium core allows comparison of depletion characteristics and shutdown margin for conditions approximating typical FNR operation.

The following sections include a description of the model core configurations and a comparison of core physics parameters.

9.3.1 Description of Batch and Equilibrium Core Models

The batch core model consists of 31 fresh fuel assemblies, with four special assemblies at control rod locations. The configuration is symmetric about the north/south midplane and was analyzed using half-core calculations with a 6x6 mesh/assembly. Figure 7 illustrates this configuration.

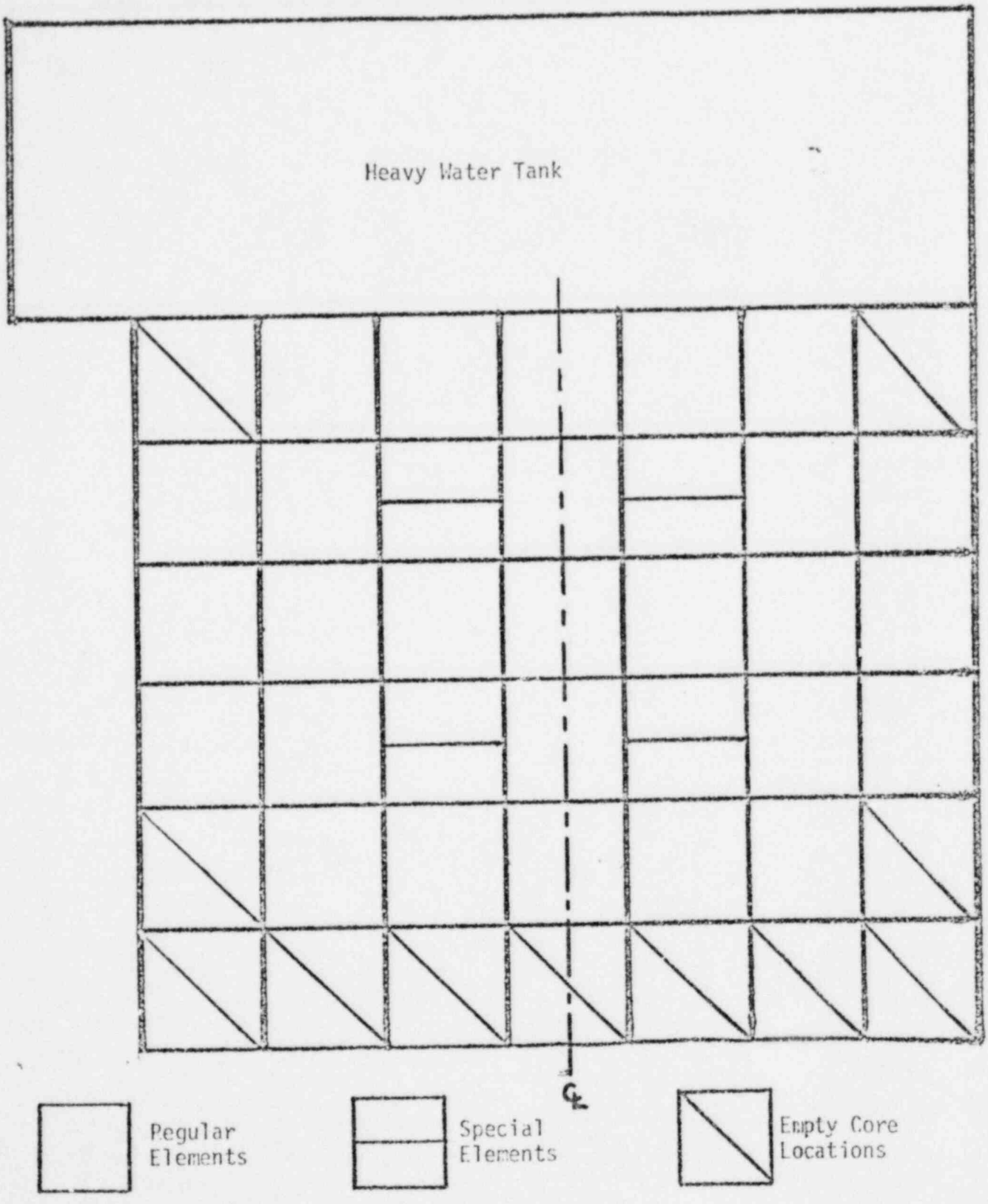

Figure 7. Batch Core Configuration

The equilibrium core configuration shown in Figure 8 essentially simulates a typical FNR shuffling pattern, and is chosen so that the core loading and shuffling patterns repeat every sixth cycle. The core configuration consists of 39 fuel elements including six special fuel elements. The important criteria for choosing the core loading pattern are:

1. Fresh fuel elements are loaded into the central region of the core. This maximizes control rod worth and helps maintain the required shutdown margin. The fuel elements are moved outward in an in/out shuffling scheme as they deplete.

2. The fuel elements are loaded so as to equalize the worths of the three shim rods. Because the B and C Rods tend to be less reactive, the reactivity worth of these shim rods is increased by loading relatively fresh fuel into the vicinity of B and C Rods. In contrast, more depleted fuel is loaded near the A Rod.

With these core loading criteria, an equilibrium core burnup distribution is obtained with 2DB calculations, which repeats cyclically over a given time period. The fuel element shuffling pattern for the equilibrium core divides the 33 regular fuel element locations into eight loading zones as shown in Figure 8. Each regular element loading zone corresponds to core locations having nearly equal fuel burnup, although not necessarily equal burnup rates. New fuel is loaded into Zone 1 and depleted fuel is discharged from Zone 8. At the start of each cycle, one new element is loaded into Zone 1, and the element in Zone 1 is moved to Zone 2. Another element is moved from Zone 2 to 3, and continuing to Zone 8, with a depleted element being discharged from Zone 8. Because the core loading zones have a maximum of six elements, the core burnup distribution repeats every sixth cycle. The eight-zone shuffling pattern for the regular elements is shown in Table 6.

The shuffling pattern for the special fuel elements is somewhat different since there are six special element locations. A new special element is added and a depleted element is discharged only every sixth cycle. With this shuffling pattern a new special element is placed in Special-Zone 1 at the start of cycle 1. The element removed from Special-Zone 1 is placed in ex-core storage for one cycle and then placed in Special-Zone 2 at the start of cycle 2. The element from Special-Zone 2 is moved to storage before being placed into Special-Zone 3 at the start of cycle 3. The sequence continues until the start of cycle 6 when the element from storage is placed into Special-Zone 6 and a depleted special element is discharged from the core. This shuffling pattern for special elements is shown in Table 7.

While the reactivity decrease and core power distribution are nearly constant over each equilibrium cycle, the burnup distribution will repeat only every sixth cycle or over one macro-cycle. Any core para-

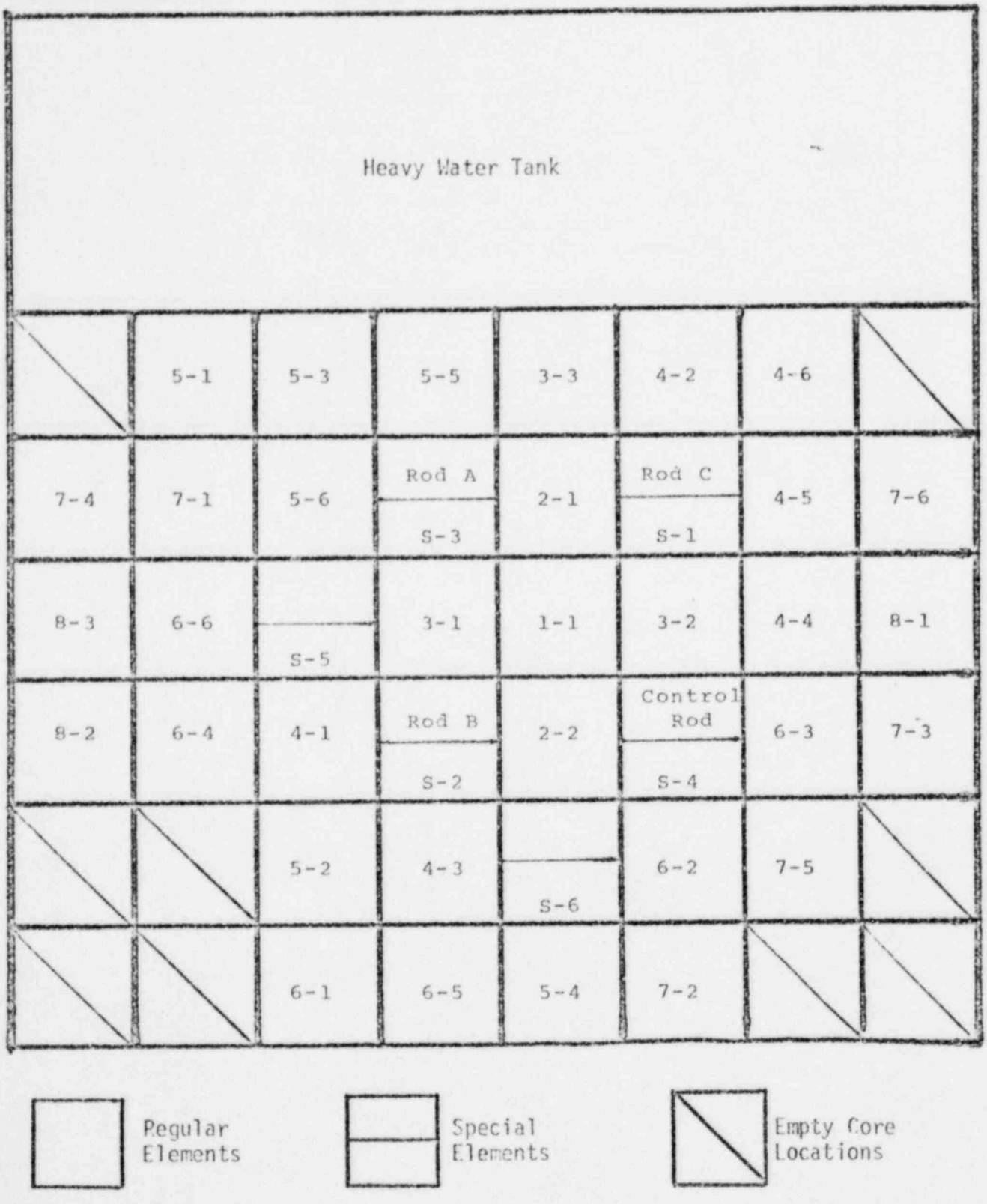

Figure 8. Equilibrium Core Loading Pattern

Table 6
Regular Fuel Element Shuffling Scheme

Equilibrium Core Configuration
with 6 Cycles/Macro-cycle

Cycle	Core Loading Zone 1	2	3	4	5	6	7	8
	New Fuel							
1	→ 1-1	→ 2-1	→ 3-1	→ 4-1	→ 5-1	→ 6-1	→ 7-1	→ 8-1 →
2	→ 1-1	→ 2-2	→ 3-2	→ 4-2	→ 5-2	→ 6-2	→ 7-2	→ 8-2 →
3	→ 1-1	→ 2-1	→ 3-3	→ 4-3	→ 5-3	→ 6-3	→ 7-3	→ 8-3 →
4	→ 1-1	→ 2-2	→ 3-1	→ 4-4	→ 5-4	→ 6-4	→ 7-4	→ 8-1 →
5	→ 1-1	→ 2-1	→ 3-2	→ 4-5	→ 5-5	→ 6-5	→ 7-5	→ 8-2 →
6	→ 1-1	→ 2-2	→ 3-3	→ 4-6	→ 5-6	→ 6-6	→ 7-6	→ 8-3 →
								↓ Discharge

Table 7

Special Fuel Element Shuffling Scheme

Equilibrium Core Configuration
with 6 Cycles/Macro-cycle

Cycle	Storage		Core Loading Zone		Storage
1	New fuel	→	S-1	→	X_1
2	X_1	→	S-2	→	X_2
3	X_2	→	S-3	→	X_3
4	X_3	→	S-4	→	X_4
5	X_4	→	S-5	→	X_5
6	X_5	→	S-6	→	Discharge

meter will be exactly the same at a given time into any macro-cycle.

To verify the practicability of the equilibrium cycle, Table 8 presents a comparison of the calculated equilibrium core parameters and actual core parameters based on the FNR operating experience during the past year. These comparisons indicate that the proposed equilibrium cycle represents a reasonably practical configuration, which may be used to compare the characteristics of the LEU and HEU designs for typical FNR operating conditions.

9.3.2 Comparison of Core Physics Parameters for HEU and Proposed LEU Fueled Cores

The major physics parameters which have been analyzed include the power defect of reactivity, xenon reactivity worth, control (shim) rod reactivity worth, cycle length, and shutdown margin. Differences in these parameters, as computed for the two model core configurations should provide a reasonable estimate of any effects of LEU fuel on FNR safety margins. These differences are compared for several equilibrium cores with differing cycle length and the batch core.

9.3.2.1 Temperature Coefficient of Reactivity and Power Defect Comparison

The isothermal temperature coefficient of reactivity was computed for the batch core model to be -8.4 pcm/°F for the HEU fuel and -12.6 pcm/°F for the LEU fuel. The large increase is due almost exclusively to fuel Doppler effects. For the HEU fuel, fuel Doppler effects are negligible due to the small amount of ^{238}U present. For the LEU fuel, the large amount of ^{238}U increases resonance absorptions in ^{238}U, resulting in much larger sensitivity to fuel temperature. The principal contribution to temperature coefficient of reactivity for both the HEU and LEU configurations is the effect of the reduction in moderator density on leakage and moderation.

The power defect of reactivity represents the total of all reactivity effects induced by taking the reactor from a cold zero-power condition to normal operating conditions. Due to the spatially nonuniform temperature and density changes involved, the power defect cannot be predicted solely on the basis of an isothermal temperature coefficient. Since the increased fuel Doppler effect is, however, the principal difference in the temperature effects between the HEU and the LEU designs, the change in power defect of reactivity is estimated in the present analysis on the basis of calculated temperature coefficients. Based on an average core temperature rise of 7°F, the power defect for the LEU fuel is estimated to be about .03% $\Delta k/k$ larger in magnitude than for HEU fuel. For a typical FNR configuration, the excess reactivity required to overcome the power defect would thus change from a measured value of .21% $\Delta k/k$ for HEU to .24% $\Delta k/k$ for LEU.

Table 8

Comparison of the Equilibrium Core Parameters with the Actual FNR Parameters

	Equilibrium Core 93% Enrichment	FNR Experience (Oct. 78 - Sept. 79)
Average cycle length (days)	11	8.17*
Average reactivity swing between shuffles (% Δk/k)	-0.31	-0.40
Average number of shuffles/day	0.82	0.81
Average discharge burnup (%)		
Regular elements	17	17
Special elements	29	34
Calculated k_{eff}		
Range	1.022 ~ 1.026	1.020 ~ 1.032
Average	1.024	1.025
Control Rod Worth (% Δk/k)	(at beginning of cycle)	(at beginning of Cycle 67)
Shim Rod A	2.21	2.22
Shim Rod B	2.20	2.11
Shim Rod C	2.00	1.72
Total	6.41	6.05

*Includes periods of operation at 1MW power.

9.3.2.2 Xenon Reactivity Worth Comparison

The xenon reactivity worths for the LEU and HEU equilibrium core configurations are compared in Table 9 and in Table 10 for the batch cores. For the cases considered the xenon worth is slightly lower for the LEU than the HEU fuel. There are two competing effects responsible for this decrease: First, the larger ^{235}U loading for the LEU core results in lower in-core thermal flux levels, with a greater (10-12%) xenon concentration. Second, the increased ^{235}U loading gives the LEU core a larger neutron absorption cross-section. As total core absorption is increased, the fractional absorption in xenon, and thus the xenon reactivity worth, is decreased. Although these two effects tend to cancel one another, the latter effect dominates and xenon reactivity worth is lowered by about .1% $\Delta k/k$.

9.3.2.3 Control Rod Reactivity Worth Comparison

A comparison of the reactivity worths for shim rods A, B, and C is given in Table 9 for equilibrium cores and in Table 10 for batch cores. As expected, the rod worth is lower for the LEU cores. The greatest loss in total rod worth, .33% $\Delta k/k$, is seen for a batch core comparison. For the equilibrium cores, comparing the HEU regular cycle with the LEU cycle corresponding to an equal reactivity change shows a decrease of total rod worth of only .08% $\Delta k/k$, indicating that larger core-average burnup in the LEU core can mitigate the decrease in rod worth for the LEU core.

The decrease in rod worth is an expected result of the increased ^{235}U loading required for LEU fuel. When the loading of the principal core absorber (^{235}U) is increased, the control rods become less effective in competing with fuel for neutron absorption and the rod worth is decreased. Accordingly, fuel depletion should increase control rod effectiveness. This prediction is borne out by the equilibrium core calculations displayed in Table 9 and suggests that a longer LEU cycle could provide a means for increasing both control rod reactivity worth and shutdown margin.

9.3.2.4 Comparison of Depletion Characteristics

Depletion effects on reactivity for several equilibrium-core cycle lengths are presented in Table 9. Comparing the 11-day cycle for HEU and LEU cores shows that for equal cycle lengths, the rate of reactivity loss due to fuel burnup is 25% ~ 30% lower for the LEU core. This is primarily a direct consequence of the increased ^{235}U loading - for a given absolute loss of fuel mass, the fractional depletion and its reactivity loss are decreased for higher fuel loading. In addition there is a secondary contribution due to the build-up of ^{239}Pu. While the reduction in the rate of reactivity decrease seen for equal length cycles would reduce the excess reactivity requirement, the reduction in control rod worth could result in a net decrease in shutdown margin. Another consequence of the equal-length fuel cycle is that fuel element discharge burnup is reduced, thus likely increasing fuel costs.

Table 9

Core Physics Parameters for Equilibrium Core

	HEU		LEU		
	Regular	Extended	Equal Length	Equal Burnup	Equal Reactivity change
Cycle length (days)	11.0	13.0	11.0	13.0	15.0
Average discharge burnup (MWD/assembly)	19.2	22.8	18.6	21.8	25.3
Core average burnup at beginning of cycle (MWD/assembly)	10.7	12.6	10.6	12.6	14.6
Average reactivity change/cycle (% Δk/k)	- 0.31	- 0.38	- 0.23	- 0.26	- 0.32
Shim rod worth (% Δk/k)					
A Rod	2.21				2.20
B Rod	2.20				2.18
C Rod	2.00	2.06	1.82	1.86	1.95
Total	6.41				6.33
Excess reactivity required (% Δk/k)					
Xenon poisoning	2.24				2.08
Burnup effect	0.31				0.32
Power defect	0.21				0.24
Total	2.76				2.64
Shutdown margin (% Δk/k)	3.65				3.69

Table 10

Core Physics Parameters for Batch Core

	HEU	LEU
Cycle length (days)	10.0	10.0
Reactivity change per cycle (% Δk/k)	- 0.31	- 0.22
Shim rod worth (% Δk/k)		
A Rod	2.37	2.26
B Rod	2.23	2.12
C Rod	2.37	2.26
Total	6.97	6.64
Excess reactivity required (% Δk/k)		
Xenon poisoning	2.50	2.40
Burnup effect	0.31	0.22
Power defect	0.21	0.24
Total	3.02	2.86
Shutdown margin (% Δk/k)	3.95	3.78

Since control rod worth calculations predict an increase in rod worth as fuel burnup is increased, two extended length cycles were investigated for LEU fuel: The first, with a length of 13 days, is intended to match fuel burnup with the 11-day HEU cycle. The second, with a length of 15 days, is intended to yield the same reactivity change per cycle as the 11-day HEU cycle. Results obtained for the two extended LEU cycles, as well as an extended HEU cycle for comparison, are included in Table 9.

Comparison of the 15-day LEU cycle with the 11-day HEU cycle shows that the fuel element discharge burnup is increased by 30%, and the cycle length is increased by 36%, while maintaining approximately equal reactivity change/cycle. These considerations suggest that fuel utilization is expected to be better for LEU fuel and that, over a long period of time, fuel costs could be lowered. This improvement in fuel utilization can be attributed to the small fissile plutonium buildup, increased fast fission due to ^{238}U, and spectrum hardening which reduces the reactivity effects of fuel depletion.

The most important consequence, however, of the extended 15-day LEU cycle is the effect on control rod reactivity worth. The extended cycle length increases the rod worth to a value approximately equal to the regular 11-day HEU cycle.

Since the 15-day LEU cycle offers distinct advantages over the 11- or 13-day LEU cycles, it has been analyzed in detail. Succeeding comparisons of LEU and HEU equilibrium core models will therefore compare the 11-day HEU cycle with the 15-day LEU cycle.

9.3.2.5 Comparison of Shutdown Margin

The most significant safety parameter related to core physics analysis is the shutdown margin. This parameter is obtained by subtracting the positive core excess reactivity required to overcome xenon poisoning, fuel depletion, and the power defect from the total control rod reactivity worth. The present Technical Specifications require that the shutdown margin be at least 3.0% $\Delta k/k$. Any difference between the estimated shutdown margin and the limiting value represents excess reactivity available for experiments.

For the LEU batch core, it is seen from Table 10 that the lower excess reactivity requirement is overshadowed by the decrease in control rod reactivity worth. The shutdown margin of 3.78% $\Delta k/k$ is lower than for the HEU core, but is still well above the 3% $\Delta k/k$ requirement. Additionally, with the most reactive rod fully withdrawn, the shutdown margin is 1.52% $\Delta k/k$, well in excess of the .75% $\Delta k/k$ required.

Comparing the HEU and LEU equilibrium core results shown in Table 9, it is seen that for cycles having equal reactivity change, the shutdown margin for the LEU core exceeds that

for the HEU core. This rather surprising result is a consequence of the longer cycle length and a higher average fuel burnup in the LEU equilibrium core. With the HEU and LEU control rod worths nearly equalized, the relatively minor effect of lower xenon poisoning increases the shutdown margin slightly. The computed value of 3.69% $\Delta k/k$ is well in excess of the 3.0% $\Delta k/k$ requirement. Also, the shutdown margin with the most reactive control rod fully withdrawn in 1.49% $\Delta k/k$, well above the .75% $\Delta k/k$ required.

9.3.3 Comparison of Flux and Power Distributions

Calculated power distributions for both HEU and LEU cores are compared in Figures 9 and 10 for batch cores and equilibrium cores, respectively. Examination of these figures reveals only minor changes between LEU and HEU cores. The largest change in assembly power, a 3% relative increase, occurs for special element locations. Additionally, there is a small shift in the power distribution away from the heavy water tank and toward a slightly improved overall symmetry about the center. There is no evidence of changes which would require detailed thermal-hydraulic analysis; in fact, the ratio of peak to average assembly power is slightly reduced.

The calculated thermal flux distributions are compared in Figure 11 for batch cores and Figure 12 for equilibrium cores. A major difference between HEU and LEU fuel is apparent from these figures: since for a well moderated core the power is approximately proportional to the product of the macroscopic fission cross-section and thermal flux, an increased fuel loading results in a corresponding reduction in thermal flux for a given power. This effect is readily apparent in Figures 11 and 12, where the thermal flux in regular fuel elements is seen to decrease by about 14%. For special fuel elements, the reduction in thermal flux is only about 9%. This mitigation in the thermal flux decrease results from the effect of the thermal flux peaking in the large waterhole. This peak is primarily dependent on the fast flux, which is not significantly different between the LEU and HEU fuels. Since the thermal flux level within the special element will be affected by the waterhole peaking, the overall effect is to mitigate the decrease in thermal flux. As noted for the power distribution, there is a slight shift in thermal flux away from the heavy water tank toward a slightly improved overall symmetry about the center. Figures 13 and 14 display thermal flux for traverses along the north-south core center lines. It should be noted that the centerline of the equilibrium core is bordered by two special assemblies, whereas the batch core centerline is through the centers of regular assemblies. The general reduction in thermal flux is apparent in both figures, and the mitigating effects of the special assemblies are evident in the equilibrium core traverse.

Calculations of the ex-core thermal flux in the heavy water tank have indicated that the thermal leakage flux will be reduced by 6~10%. While this is an important consideration for experimental usage, it has no impact on the core safety analysis.

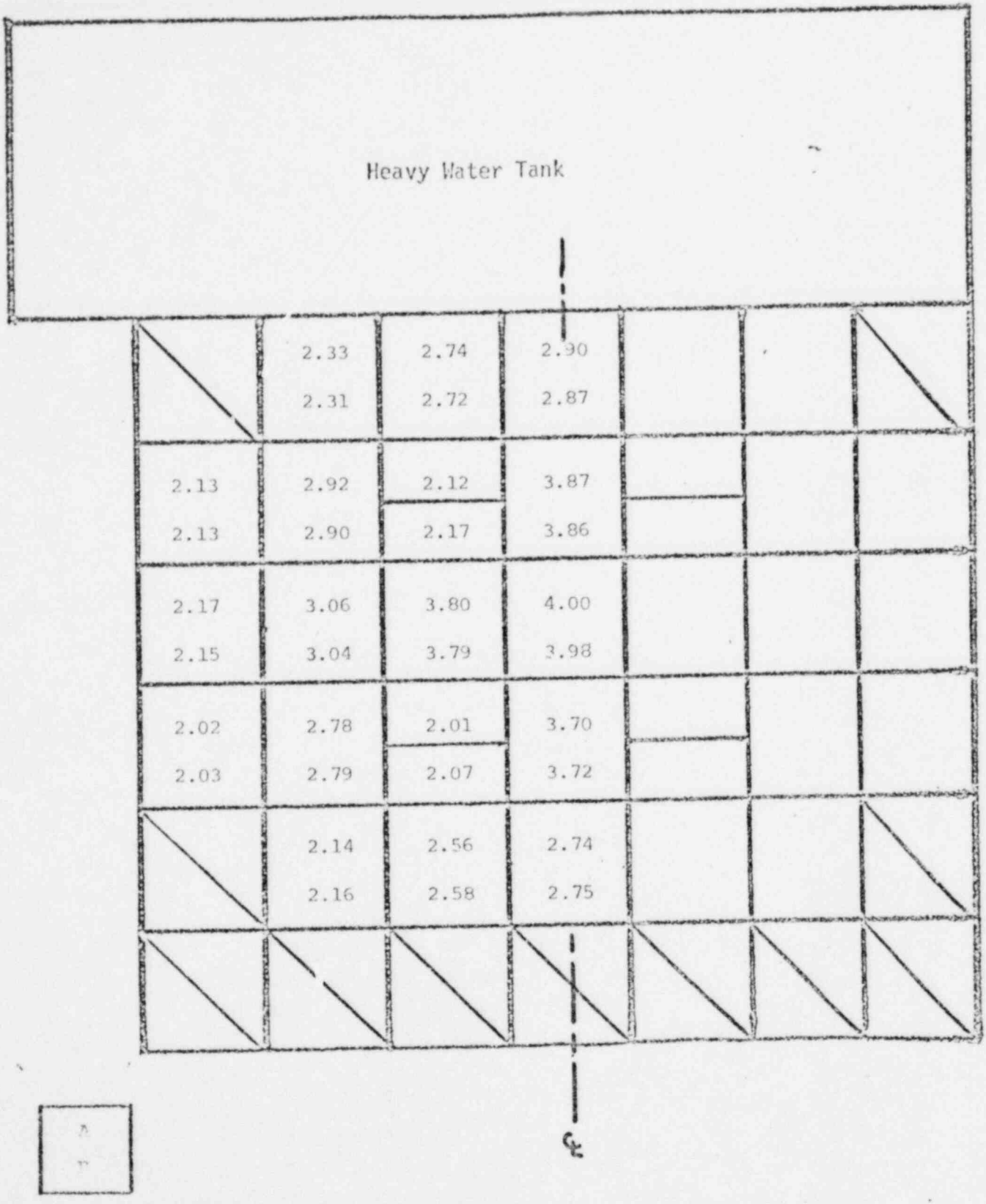

A: Assembly Power (%), HEU Core

B: Assembly Power (%), LEU Core

Figure 9. Assembly Power Distribution for Batch Core

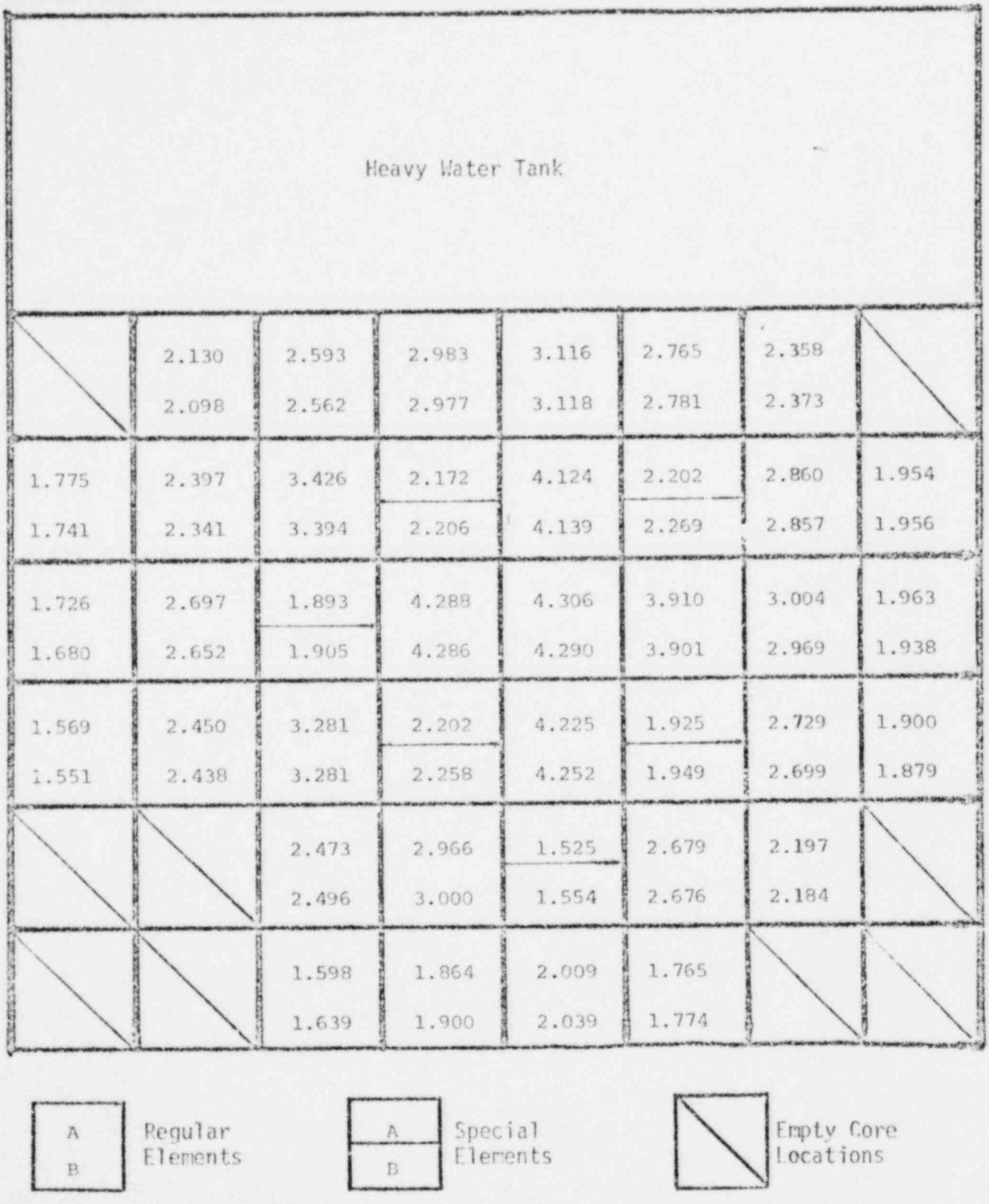

Figure 10. Assembly Power Distribution for Equilibrium Core

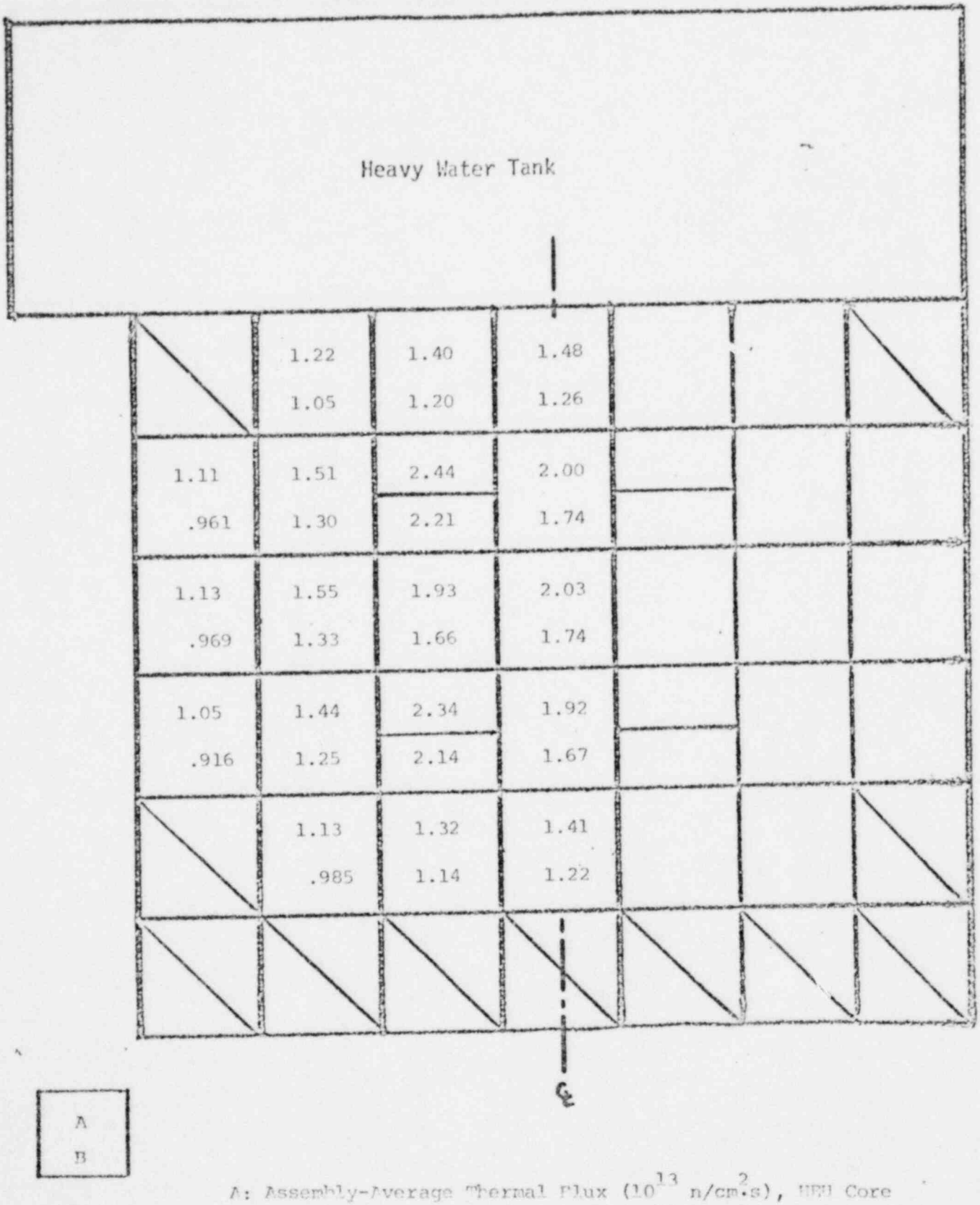

A: Assembly-Average Thermal Flux (10^{13} n/cm^2·s), HEU Core

B: Assembly-Average Thermal Flux (10^{13} n/cm^2·s), LEU Core

Figure 11. Assembly-Average Thermal Flux Distribution for Batch Core

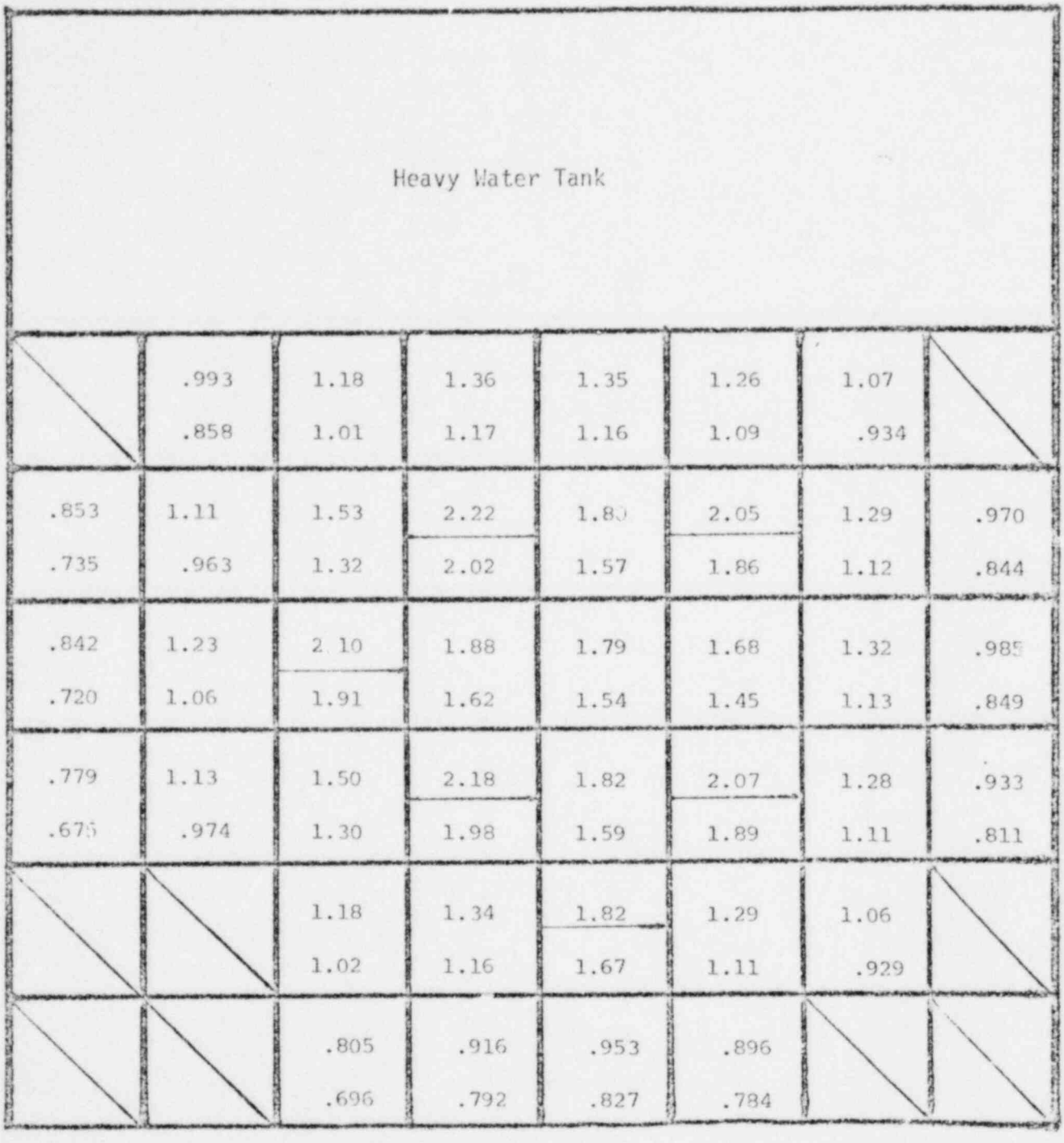

A: Assembly Average Thermal Flux (10^{13} n/cm^2·s), HEU 11-day Cycle

B: Assembly Average Thermal Flux (10^{13} n/cm^2·s), LEU 15-day Cycle

Figure 12. Assembly-Average Thermal Flux Distribution for Equilibrium Core

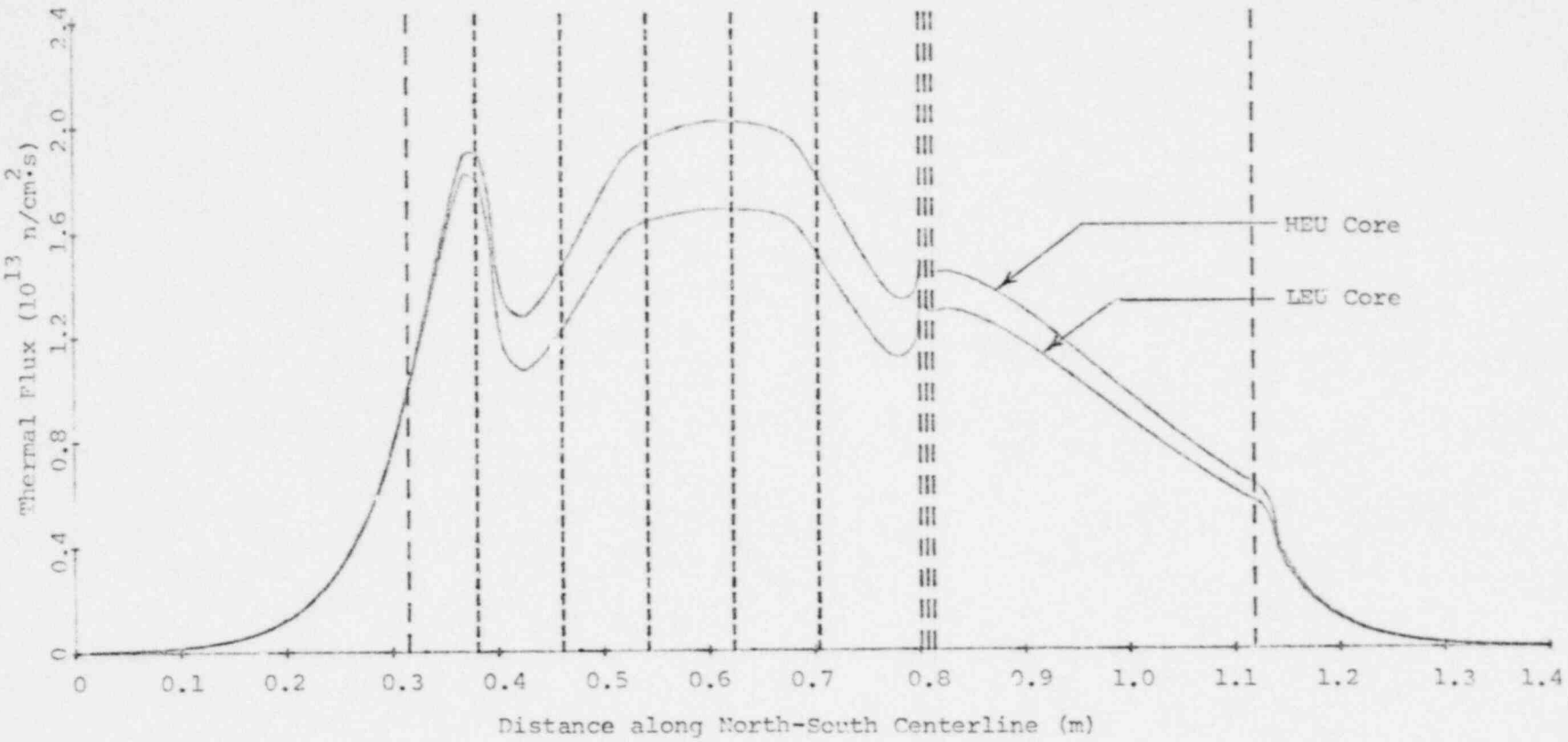

Figure 13. Thermal Flux Distribution for Batch Core

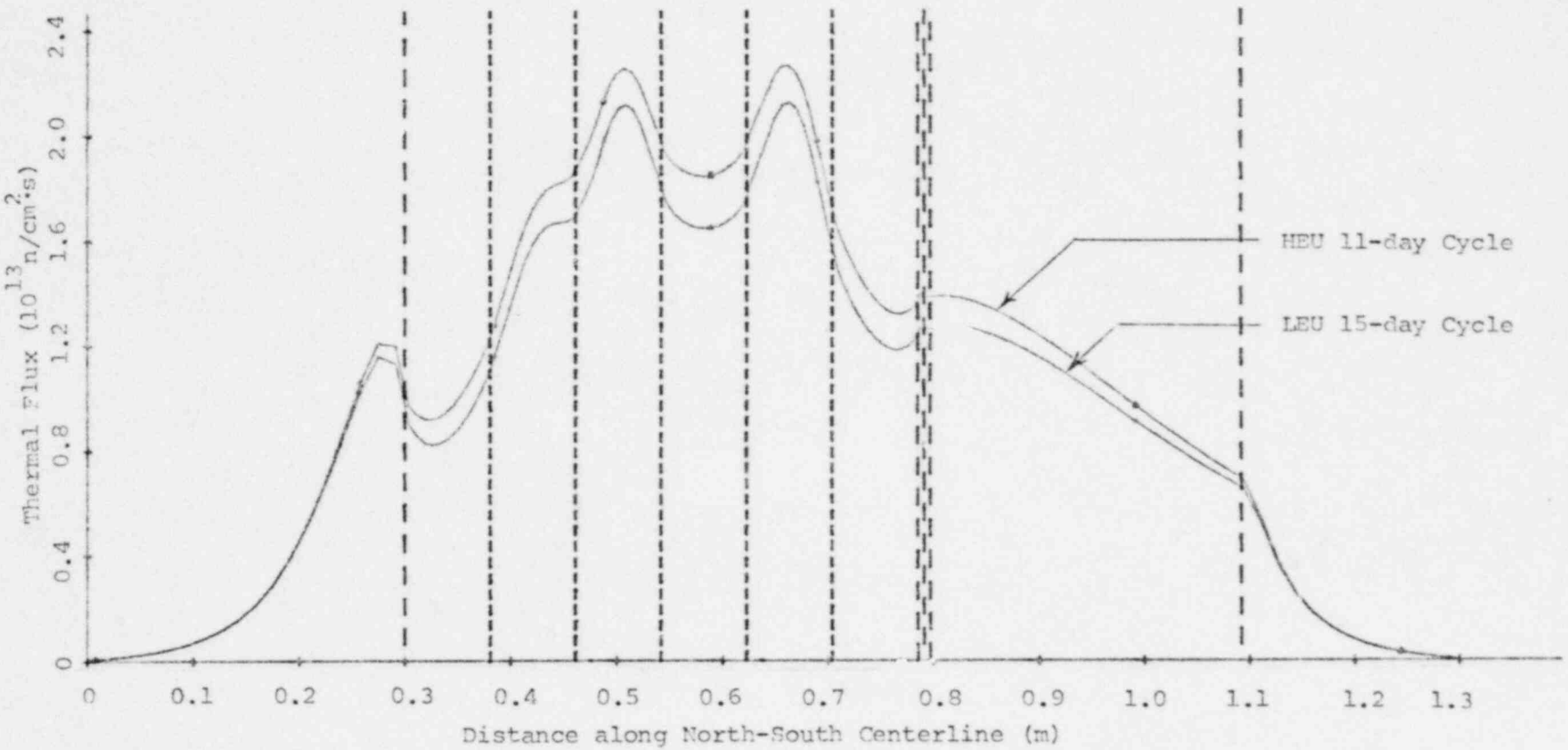

Figure 14. Thermal Flux Distribution for Equilibrium Core

9.3.4 Core Dynamic Characteristics

Of the physics parameter changes that would affect core dynamics, temperature coefficient and power defect, which is largely affected by temperature coefficient, are expected to be the parameters of greatest significance. Calculations indicate the magnitude of negative temperature coefficient increases from -8.4 pcm/°F to -12.6 pcm/°F, primarily due to ^{238}U Doppler. The transient safety characteristics of the core are expected to improve because of the larger negative temperature coefficient and power defect.

The calculated slight decrease in total rod worth still allows for shutdown margins well in excess of Technical Specification limits and sufficient excess reactivity for normal cycle operations. These and other core physics parameters will be verified in the demonstration experiment and measurement program.

The FNR Safety Limits and Limiting Safety System Settings are designed to ensure that fuel clad integrity is maintained. They are based on static combinations of reactor power, core inlet temperature, coolant flow rate, and pool height which prevent boiling in the hottest spot in the core. These limits and settings are not altered by the changes in core physics parameters.

9.4 Summary of the Core Physics Analysis

Extensive effort has been devoted to the development of accurate calculational methods for the analysis of HEU and LEU fueled research reactors. These methods make use of existing well-verified computer codes wherever possible and have been verified through comparison with data from several different research reactor configurations. The accuracy of the computational methods is expected to be equally valid for the prediction of changes in core physics parameters due to the use of LEU fuel. To encompass all expected effects of the proposed LEU fuel, both a batch core model and an equilibrium core model were analyzed in detail and compared with the HEU fuel. The results of these comparisons serve to quantify predictions which can be made on physical grounds: decreasing the fuel enrichment from 93 w/o to 19.5 w/o and increasing the ^{235}U loading from 140 grams to 167.3 grams per 18-plate assembly result in a large decrease in the in-core thermal flux; a small decrease in xenon poisoning; a small increase in power defect due to increased Doppler effects; longer cycle length for a given reactivity change and higher discharge fuel burnup; a reduction in control rod worth, which may be offset by longer cycle; very little change in power distribution; and, most importantly, no significant change in the core shutdown margin.

While there are changes in core physics parameters for the proposed LEU fuel, there appear to be no reductions in any safety margins.

10. DEMONSTRATION EXPERIMENT AND MEASUREMENT PROGRAM

The demonstration experiments and measurements program will: 1) characterize the FNR in sufficient detail to discern and quantify neutronic differences between high and low enrichment cores, and 2) provide measurements to benchmark core physics calculations.

The experiments chosen to accomplish this program are:

1. Wire activation measurements to provide absolute flux normalization.
2. Rhodium detector flux maps to provide absolute thermal (in-core and ex-core) fluxes.
3. Neutron diffraction measurements to determine the flux spectrum in the D_2O reflector.
4. Control rod worth measurements and power defect measurements.
5. Unfolding of foil activation measurements to determine the in-core flux spectrum.

10.1 Analysis of the Current High Enrichment Uranium Core

Experimental and analytical efforts are in progress which are designed to characterize the present FNR core. Spatial flux distributions are being measured with ^{103}Rh movable self-powered neutron detectors, with proper correction factors applied for epithermal neutrons. The measurement of fast neutron spectra are being made using the multiple threshold foil technique and the unfolding calculations (SAND-II and modified SAND-II codes) will be performed. In-core thermal flux spectra are being measured by standard activation foil techniques and Cd ratio methods, and the leakage spectra by crystal spectrometer method. In-core flux, correlated to changes in the reactor core configurations, is being measured by partial-core ^{103}Rh flux maps and the leakage neutron flux levels in beam ports in preparation for partial loading of low-enrichment fuel elements. In addition, measurements of other reactor parameters including control rod worth and reactivity coefficients will be performed. We will also establish, to the extent possible, the accuracy of our measurement techniques so that we can obtain meaningful comparison between the high- and low-enrichment fuels and also with the calculated results.

10.2 Testing and Measurements on the Low-Enrichment FNR Core

Detailed measurements of flux distribution and other reactor parameters for partial- and full-core low-enrichment configurations of the FNR core will be performed. The measurements will be performed in accordance with the techniques established in section 10.1. The need for any modifications in the measurement techniques or detector calibrations for the low-enrichment environment will be determined prior to the full-core loading. The measurements will include in-core and ex-core maps, spectra, and other standard reactor physics parameters.

REFERENCES

1. G.W. Gibson, "The Development of Powdered Uranium Aluminide Compounds for Use as Nuclear Reactor Fuels," IN-1133, TID-4500, Idaho Nuclear Corporation, December, 1967.

2. R.M. Brugger, "Metallurgy and Materials Science Branch Annual Report Fiscal Year 1970", IN-1437, Idaho Nuclear Corporation, November, 1970.

3. R.R. Hobbins, "INC-16-2 Irradiation Experiment", Idaho Operations Office, U.S. Atomic Energy Commission, July 19, 1974.

4. M.M. Martin, A.E. Richt, and W.R. Martin, "Irradiation Behavior of Aluminum Base Fuel Dispersions," ORNL-4856, Oak Ridge National Laboratory, May, 1973.

5. W. Dienst, S. Nazare, and F. Thummber, "Irradiation Behavior of UAl_x Dispersion Fuels for Thermal High Flux Reactors," Journal of Nuclear Materials, 64, 1977.

6. W.C. Francis, ANNUAL PROGRESS REPORT OF REACTOR FUELS AND MATERIALS DEVELOPMENT FOR FY 1965, USAEC Report IDO-17154, Idaho Operations Office, U.S. Atomic Energy Commission, February, 1966.

7. G.W. Gibson, M.J. Graber, V.A. Walker, and W.C. Francis, "Results of ATR Sample Fuel Plate Irradiation Experiment", IDO-16958, Idaho Operations Office, U.S. Atomic Energy Commission, March 23, 1964.

8. D.J. Rucker, "Fuels and Materials Development Program Quarterly Progress Report for Period Ending March 31, 1970", ORNL-4560, Oak Ridge National Laboratory, March, 1970.

9. "Reactor Safety Evaluation of ORNL Proposal to Modify Fuel in ORR", Oak Ridge National Laboratory, February, 1977.

10. P. Tichler, "Review of Proposed Increase in Fuel Element Loading and Fuel Burnup", Memorandum,Brookhaven National Laboratory, February, 1977.

11. V.A. Walker, M.J. Graber, and G.W. Gibson, "ATR Fuel Materials Development Irradiation Results - Part II," IDO-17157, Idaho Operations Office, U.S. Atomic Energy Commission, June, 1966.

12. R. F. Barry, "LEOPARD - A Spectrum Dependent Non-spatial Depletion Code", WCAP-3269-26, Westinghouse Electric Corporation (September 1963).

13. J. Barhen, W. Rothenstein. E. Taviv, "The HAMMER Code System", NP-565, Electric Power Research Institute (October 1978).

14. W. W. Little, Jr. and R. W. Hardie, "2DB User's Manual-Revision I", BNWL-831 REV1, Battelle Pacific Northwest Laboratory (February 1969).

15. W. W. Engle, Jr., "A User's Manual for ANISN, a One-Dimensionsl Discrete Ordinates Transport Code with Anisotropic Scattering", K-1693, Oak Ridge Gaseous Diffusion Plant (March 1967).

16. K. D. Lathrop and F. W. Brinkley, "TWOTRAN-II - An Interfaced Exportable Version of the TWOTRAN Code for Two-Dimensional Transport", Los Alamos Scientific Laboratory, LA-4848-MS (1973).

17. D. R. Vondy, T. B. Fowler, and G. W. Cunningham, "VENTURE: A Code Block for Solving Multigroup Neutronics Problems Applying the Finite-Difference Diffusion Theory Approximation to Neutron Transport", ORNL-5062 (1975).

18. M. H. Theys, "Integral Transport Theory of Thermal Utilization Factor in Infinite Slab Geometry", Nucl. Sci. Eng., 7, 58 (1960).

19. S. Jabbawy, J. Karni, W. Rothenstein, and S. Velner, "Water Moderated Reactor Analysis with ENDF/B Data", Nuclear Data in Science and Technology, Vol. II, p. 147, IAEA, Vienna (1973).

20. N. G. Demas, "Representation of Two-Dimensional Self-Shielded Poison Lumps in P-1 Calculations", WAPD-BT-21, Westinghouse Electric Corporation, pp. 29-32 (Nov. 1960).

21. E. B. Johnson, "Power Calibration for BSR Loading 33", CF-57-11-30, Oak Ridge National Laboratory (1957).

22. J. M. Hendrie, "Final Safety Analysis Report on the Brookhaven High Flux Beam Research Reactor", BNL-7661, Brookhaven National Laboratory (April 1964).

23. R.R. Burn, "Research, Training, Test, and Production Reactor Directory", United States of America, Order No. 250001, American Nuclear Society, LaGrange Park, Illinois, 1980.

BIBLIOGRAPHY

1. G.M. Adamson, "Fabrication of Research Reactor Fuel Elements", ORNL-TM-2197, Oak Ridge National Laboratory, June 1968.

2. ALCOA ALUMINUM HANDBOOK, Aluminum Company of America, Pittsburgh, 1962.

3. HANDBOOK OF ALUMINUM, Alcan Aluminum Corporation, Cleveland, 1970.

4. D.M. Alger and C. Julian, "UAl_x Fuel in Research Reactors", Transactions of the American Nuclear Society, Chicago, June 10-14, 1973.

5. C. Allain, H. Aubert, and J. Laniesse, "Irradiation Dans Le Reacteur El 3 De Tubes En Uranium Faiblement Allie", Journal of Nuclear Materials, 31, Number 2, June 1969.

6. ALUMINUM WITH FOOD AND CHEMICALS, The Aluminum Association, New York, February 1969.

7. ALUMINUM STANDARDS AND DATA, The Aluminum Association, New York, December, 1969.

8. W.E. Berry, CORROSION IN NUCLEAR APPLICATIONS, John Wiley and Sons, New York, 1971.

9. J.H. Buddery, M.E. Clark, R.J. Pearce and J.J. Stobbs, "The Development and properties of an Oxidation-Resistant Coating for Uranium", Journal of Nuclear Materials, 13, No. 2, 1964.

10. B.L. Bramfitt and H.P. Leighly, "A Metallographic Study of Solidification and Segregation in Cast Aluminum-Uranium Alloys", Metallography, Vol. 1, No. 2, November 1968.

11. R.M. Brugger, "Metallurgy and Materials Science Branch Annual Report Fiscal Year 1970", IN-1437, Idaho Nuclear Corporation, November 1970.

12. J. Chamberlain, M.P. Johnson, J.R. Kench and A.G. Young, "The Influence of Microstructure on the Behaviour of Uranium Alloys During Temperature Cycling Creep Experiments", Journal of Nuclear Materials, 19, No. 2, 1966.

13. A.K. Chakraborty, R.S. Crouse and W.R. Martin, "Factors Affecting the Swelling During Degassing of Compacts Containing Uranium-Aluminum Inter-Metallics Dispersed in Aluminum", ORNL-TM-2800, Oak Ridge National Laboratory, March 1970.

14. P. Chiotti and J.A. Kateley, "Thermodynamic Properties of Uranium-

Aluminum Alloys", Journal of Nuclear Materials, 32, No. 1, August 1969.

15. J.K.Dawson and R.G. Sowden, CHEMICAL ASPECTS OF NUCLEAR REACTORS, Butterworth and Co., London, 1963.

16. D.R. deBoisblanc, "Reactor Engineering Branch Annual Report Fiscal Year 1968", IN-1228, Idaho Nuclear Corporation, February 1969.

17. D.R. deBoisblanc, "Reactor Engineering Branch Annual Report Fiscal Year 1969", IN-1335, Idaho Nuclear Corporation, November 1969.

18. D.R. Dickinson, R.J. Lobsinger and R.B. Richman, "Corrosion of Aluminum-Clad Fuel Elements", TID-7642, Research Reactor Fuel Element Conference, Gatlinburg, Tennessee, September 1962.

19. W. Dienst, S. Nazare, F. Thummler, "Irradiation Behavior of UAl_x-Al Dispersion Fuels for Thermal High Flux Reactors", Journal of Nuclear Materials, 64, 1977.

20. J.O. Dittmer, "A Study of the Compressive Properties of Aluminum Clad Composite Nuclear Reactor Fuel Plates", Master's Thesis, Idaho State University, 1969.

21. E.A. Eldridge and H.W. Deem, "Report on Physical Properties of Metals and Alloys from Cryogenic to Elevated Temperatures", ASTM Special Technical Publication No. 296, American Society for Testing Materials, Philadelphia, April 1961.

22. H.E. Exner and G. Petzow, "Untersuchungen zur Stabilisierung von UAl_3 in Aluminiumreichen Kernbrennstoffen", Metal, No. 3, March 1969.

23. J.D. Fleming and J.W. Johnson, "Aluminum-U_3O_8 Exothermic Reactions", TID-7642, Research Reactor Fuel Element Conference, Gatlinburg, Tennessee, September 1962.

24. W.C. Francis, G.W. Gibson and W.P. Scarrah, "Some Results of Uranium Irradiations at the MTR/ETR", TID-7642, Research Reactor Fuel Element Conference, Gatlinburg, Tennessee, September 1962.

25. W.C. Francis, "Fuel Elements for Thermal Test Reactors - Performance at NRTS", AEC - Industry Meeting on Water Reactor Fuel Element Technology, Germantown, Maryland, January 1968.

26. FUEL ELEMENT FABRICATION, Volume 2, Proceedings of a Symposium in Vienna, Academic Press, New York 1961.

27. G.W. Gibson and D.R. deBoisblanc, "Uranium-Aluminum Alloy Powders for

use as Nuclear Reactor Fuels", CONF-339-5, U.S. Atomic Energy Commission, October 1963.

28. G.W. Gibson, M.J. Graber, V.A. Walker and W.C. Francis, "Results of ATR Sample Fuel Plate Irradiation Experiment", IDO-16958, Idaho Operations Office, U.S. Atomic Energy Commission, March 23, 1964.

29. G.W. Gibson, "The Development of Powdered Uranium-Aluminide Compounds for use as Nuclear Reactor Fuels", IN-1133, Idaho Nuclear Corporation, December 1967.

30. J.C. Griess, H.C. Savage, J.G. Rainwater, J.L. English and T.H. Mauney, "The Corrosion of Aluminum Alloys Under Simulated ATR and HFIR Conditions", TID-7642, Research Reactor Fuel Element Conference, Gatlinburg, Tennessee, September 1962.

31. M.J. Graber, G.W. Gibson and W.C. Francis, "Annual Progress Report on Reactor Fuels and Materials Development for FY 1963", IDO-16934, Idaho Operations Office, U.S. Atomic Energy Commission, November 25, 1963.

32. M.J. Graber, W.F. Zelezny and G.W. Bison, "Annual Progress Report on Reactor Fuels and Materials Development for FY 1964", IDO-17037, Idaho Operations Office, U.S. Atomic Energy Commission, November 1964.

33. M.J. Graber and R.A. Moen, "The Effects of Compatibility on the Performance of Aluminum Fuel Plates Containing Various Fuel Dispersions", Transactions of the American Nuclear Society, Gatlinburg, Tennessee, June 21-24, 1965.

34. D.H. Gurinsky and G.J. Dienes, NUCLEAR FUELS, D. Van Nostrand Co., New York, 1956.

35. L.J. Harrison, "Mechanical Failures of MTR Fuel Assemblies", Nucleonics, Volume 21, No. 10, October 1963.

36. L.J. Harrison, "Heat Transfer from an Aluminum/Uranium Fuel Plate in a Subcooled Pool During a TREAT Transient", Transactions of the American Nuclear Society, Seattle, June 15-19, 1969.

37. H.H. Hausner and J.F. Schumar, NUCLEAR FUEL ELEMENTS, Reinhold Publishing Corp., New York, 1959.

38. R.R. Hobbins and M.J. Graber, "ATR Extended Burnup, XA003F Results and INC-16-1 Review", Idaho Operations Office, U.S. Atomic Energy Commission, 1974.

39. R.R. Hobbins, "INC-16-2 Irradiation Experiment", Idaho Operations Office, U.S. Atomic Energy Commission, July 19, 1974.

40. R.O. Ivins, "A Study of the Reaction of Aluminum Uranium Alloy Fuel Plates

with Water Initiated by a Destructive Reactor Transient", CONF-39-70, U.S. Atomic Energy Commission, February 1963.

41. M. Jovanovic, "The Isothermal Growth of Secondary-Phase Particles in a Dilute Uranium Alloy", Journal of Nuclear Materials, 35, No. 2, May 1970.

42. C. Julian, "Evaluation of a 6.2 Kilogram U^{235} Core Loading for the Missouri University Research Reactor", University of Missouri, July 28, 1970.

43. A.R. Kaufmann, NUCLEAR REACTOR FUEL ELEMENTS, METALLURGY AND FABRICATION, John Wiley and Sons, New York, 1962.

44. R.T. King, E.L. Long, J.O. Stiegler and K. Farrell, "High Neutron Fluence Damage in an Aluminum Alloy", Journal of Nuclear Materials, 35, No. 2 May 1970.

45. J.H. Kittel, A.P. Gavin, C.C Crothers and R. Carlander, "Performance of Aluminum-Uranium Alloy Fuel Plates Under High Temperature and High Burnup Conditions", TID-7642, Research Reactor Fuel Element Conference, Gatlinburg, Tennessee, September 17-19, 1962.

46. D. Lazarevic, "Influence of Neutron Radiation on the Phase Composition of Low-Alloyed Uranium", RADIATION DAMAGE IN REACTOR MATERIALS, Volume 2, International Atomic Energy Agency, Vienna, June 1969.

47. J. Lehmann, P. Paoli and N. Azam, "Gonflement D'Alliages D'Uranium sous Irradiation", Journal of Nuclear Materials, Vol. 26, No. 2, May 1968.

48. J. Lehmann, P. Paoli and N. Azam, "Etude du Gonflement D'Alliages D'Uranium Sous Irradiation", Journal of Nuclear Materials, Vol. 27, No. 3, September 1968.

49. W.R. Martin and J.R. Weir, "Mechanical Properties of X8001 and 6061 Aluminum Alloys and Aluminum-Base Fuel Dispersion at Elevated Temperatures", ORNL-3557, Oak Ridge National Laboratory, February 1964.

50. M.M. Martin, J.H. Erwin and W.R. Martin, "Effect of Type and Concentration of Fuel on the Void Volume in Aluminum Dispersion-Type Fuel Plates", Transactions of the American Nuclear Society, Toronto, June 10-13, 1968.

51. M.M. Martin and A.E. Richt, "Effect of Void Volume on the Irradiation Performance of Aluminum-Base Dispersion-Type Fuel Plates", Transactions of the American Nuclear Society, Seattle, June 15-19, 1969.

52. M.M. Martin and W.R. Martin, "Fabrication Voids in Aluminum-Base Fuel Dispersions", ORNL-4611, Oak Ridge National Laboratory, October 1970.

53. M.M. Martin, A.E. Richt and W.R. Martin, "Irradiation Performance of Aluminum-Base Dispersion-Type Fuel Plates", Transactions of the American Nuclear Soceity, Miami, October 17-21, 1971.

54. M.M. Martin, A.E. Richt and W.R. Martin, "Irradiation Behavior of Aluminum-Base Fuel Dispersions", ORNL-4856, Oak Ridge National Laboratory, May 1973.

55. D.L. McElroy, R.S. Graves and J.F. Moor, "Physical Properties of Two-Phase Materials Used in Fuel Plate Cores", Canadian Journal of Physics, 45, 1967.

56. D.L. McElroy, "Physical Properties of Al Cermets", Oak Ridge National Laboratory, January 5, 1971.

57. Oak Ridge Reactor, "Reactor Safety Evaluation of ORNL Proposal to Modify Fuel in ORR", Oak Ridge National Laboratory, February 1977.

58. B.E. Paige, G.W. Gibson and K.L. Rohde, "The Effect of Silicon on Fabrication and Reprocessing of Aluminum Alloy Reactor Fuels", IN-1194, Idaho Nuclear Corporation, November 1968.

59. C.F. Reinke, "Irradiation and Postirradiation Annealing of Some Aluminum-Base Fuels", ANL-6665, Argonne National Laboratory, September 1963.

60. C.F. Reinke, "Postirradiation Annealing of Some Aluminum-Base Fuels", Transactions of the American Nuclear Society, Vol. 7, No. 1, Philadelphia, June 14-17, 1964.

61. A.E. Richt, C.F. Leitten, and R.J. Beaver, "Radiation Performance and Induced Transformations in Aluminum-Base Fuels", TID-7642, Research Reactor Fuel Element Conference, Gatlinburg, Tennessee, September 1962.

62. J.A.L. Robertson, IRRADIATION EFFECTS IN NUCLEAR FUELS, Gordon and Breach, New York, 1969.

63. D.J. Rucker, "Fuels and Materials Development Program Quarterly Progress Report for Period Ending June 30, 1968", ORNL-4330, Oak Ridge National Laboratory, June 1968.

64. D.J. Rucker, "Fuels and Materials Development Program Quarterly Progress Report for Period Ending September 30, 1968", ORNL-4350, Oak Ridge National Laboratory, September 1968.

65. D.J. Rucker, "Fuels and Materials Development Program Quarterly Progress Report for Period Ending December 31, 1969", ORNL-4520, Oak Ridge National Laboratory, December 1969.

66. D.J. Rucker, "Fuels and Materials Development Program Quarterly Progress Report for Period Ending March 31, 1970", ORNL-4560, Oak Ridge National Laboratory, March 1970.

67. D.J. Rucker, "Fuels and Materials Development Program Quarterly Progress Report for Period Ending September 30, 1970", ORNL-4630, Oak Ridge National Laboratory, September 1970.

68. O.J.C. Runnalls and R.R. Boucher, "Transformations in UAl_4 and $PuAl_4$", Transactions of the Metallurgical Society of AIME, Vol. 233, No. 7, New York, September 1965.

69. P. Tichler, "Examination of Reactor Safety Implications of Increased Fuel Loading and Extended Operating Cycle at the HFBR", Brookhaven National Laboratory, February 1977.

70. F. Thummler, H.E. Lilienthal and S. Nazare, "UAl_2-Al Instead of UAl_3-Al in Fuel Element Plates for Advanced Test-Reactors", Powder Metallurgy, Vol. 12, No. 23, London, 1969.

71. K.R. Van Horn, ALUMINUM, American Society for Metals, Metals Park, Ohio, 1967.

72. H.R. Voorhees and J.W. Freeman, "Report on the Elevated-Temperature Properties of Aluminum and Magnesium Alloys", ASTM Special Technical Publication No. 291, American Society for Testing Materials, Philadelphia, October 1960.

73. J.R. Weir, J.E. Cunningham and C.J. McHargue, "Metals and Ceramics Division Annual Progress Report for Period Ending June 30, 1974", ORNL-4970, Oak Ridge National Laboratory, October 1974.

74. R.E. Wison, "Kinetics of the Molten-Aluminum/Steam Reaction by the Levitation Method", Transactions of the American Nuclear Society, Vol. 6, No. 1, Salt Lake City, June 1963.

75. V.S. Yemel'Yanov and A.I. Yevstyukhin, THE METALLURGY OF NUCLEAR FUEL, Pergamon Press, New York, 1969.

76. W.F. Zelezny, G.W. Gibson and M.J. Graber, "A Microprobe Study of the Retention of the Fussion Gas Xenon in Irradiated Uranium Fuels Dispersed in Aluminum Clad Nuclear Reactor Fuel Plates", CONF-690910, United States Atomic Energy Commission, September 1969.